Chapter 4

Study Design and Data Collection

4.1 Preface

This chapter operationalizes the methodological framework of Chapter 3 by detailing the study design and data collection strategies adopted for four integrated experiments on traffic-induced vibrations (TIV). These studies address key dimensions of TIV, including structural response, vehicle classification, vibration normalization and predictive traffic modeling.

A standardized instrumentation setup comprising tri-axial accelerometers, a custom mounting rig, LIDAR-based speed measurement and synchronized video capture was deployed across urban sites. Uniform sensor placement, signal conditioning and data synchronization protocols were followed to ensure consistency across all experiments.

The chapter outlines site configurations, sensor deployment schemes, vehicle annotation methods and preprocessing workflows. These form the empirical basis for the subsequent studies: (i) speed hump-induced vibration analysis (Chapter 5), (ii) vibration emission and equivalence metrics (Chapter 6), (iii) vibration-based vehicle classification (Chapter 7) and (iv) GPS-augmented forecasting and route optimization (Chapter 8). To-

gether, these studies bridge theoretical constructs from Chapter 3 with the real-world data essential for the modeling and machine learning frameworks developed in Chapters 5 to 8.

4.2 Instrumentation Framework

4.2.1 Accelerometer

The core sensing unit is a **tri-axial wireless accelerometer** manufactured by *01dB (ACOEM), Metravib, France*, as shown in Figure 4.1(a). The sensor captures vibrations in the X (lateral), Y (longitudinal) and Z (vertical) axes. It operates with a sampling frequency of 12.8 kHz, ensuring acceptable temporal resolution and covers a frequency range of 0.5-6 kHz to capture vehicle-induced dynamics. The sensor has a sensitivity of 100 mV/g at 24°C and a full-scale range of ±80 g, supporting high dynamic response. It maintains a signal-to-noise ratio greater than 90 dB for low electronic noise and stores output data in `.CMG` format via an integrated data logger.

The accelerometer is integrated within a portable sound level meter (SLM) unit that houses a high-capacity internal memory, GPS timestamp synchronization and real-time display. The sensor is shock-resistant, IP-rated for outdoor deployment and factory-calibrated.

4.2.2 Mounting Mechanism for Accelerometer

To ensure precise installation, a custom-designed accelerometer mounting device was developed (Figure 4.1(b)), which is currently under patent filing. The device comprises a machined steel baseplate with high flatness tolerance and a central threaded cavity for securely locking the accelerometer. It features four individually adjustable legs, each with screw-threaded ends that allow fine-tuning of height and leveling to accommodate site-specific surface variations.

In addition, the calibration and mounting performance of the device were verified in the supplier's laboratory prior to deployment. The heavy steel base, weighing approximately 8 kg, was found to introduce no additional noise in the signals. At the site, the device was hammered into the pavement to achieve firm contact, and its alignment was checked with a spirit level, ensuring error-free and repeatable vibration measurements.

After positioning, the entire assembly is gently hammered into the road pavement to achieve semi-fixed contact. A split-level gauge is then used to confirm accurate directional alignment of the accelerometer along the X, Y and Z axes. This mounting mechanism ensures stability under high-amplitude vehicle-induced vibrations while preventing misalignment and minimizing measurement error.

4.2.3 Vehicle Speed Measurement via LIDAR

Vehicle speeds were recorded using the Stalker XS LIDAR Speed Gun, a handheld, laser-based instrument designed for high-precision motion capture. It operates in Doppler mode with rapid target acquisition (0.33 s) and is suitable for use under varied environmental conditions. The XS model has a speed measurement range of 2-481 km/h with an accuracy of ±1 km/h and a working distance up to 610 meters. It features a removable, high-capacity Li-ion battery that supports operation for two or more shifts per charge and can withstand temperatures from -30°C to +60°C.

During data collection, the handheld LIDAR was operated manually from a fixed roadside position. Instantaneous and peak speeds were displayed digitally on the device and manually logged in synchronization with the vibration recording system.

4.2.4 Visual Confirmation via Indoor Wi-Fi Camera

To verify each event and record vehicle pass-by characteristics, an indoor HD camera (EZVIZ C1C 2MP Wi-Fi Camera) was used (Figure 4.1(d)). This compact yet feature-rich

device enabled manual annotation of vehicle types, axles and traffic conditions. It features a Full HD 1080p resolution (1920 × 1080), a 2.8 mm lens with 106° horizontal and 130° diagonal field of view and adaptive frame rates up to 20 fps. Additional capabilities include IR night vision with automatic IR-cut filter, two-way audio with built-in microphone and speaker and support for MicroSD cards up to 256 GB. Wireless connectivity is maintained via 2.4 GHz Wi-Fi with AP pairing.

Although designed for indoor use, the camera was securely sheltered and mounted on-site to capture high-angle footage across the test zone. Its night vision and motion detection features ensured reliable identification of vehicle categories under varying lighting conditions. The HP USB-C Essential Power Bank powered the camera to support untethered operation during field deployment, providing a stable energy supply for extended monitoring durations.

(a) Accelerometer (b) Mounting Device (c) LIDAR Speed Gun (d) Wi-Fi Camera

Fig. 4.1 Instrumentation used for vehicle-induced vibration acquisition.

4.2.5 On-Site Deployment Layout

The experimental setup was implemented at selected urban and semi-urban locations to capture vehicle-induced vibrations under free-flow traffic conditions. The field deployment consisted of synchronized instrumentation and coordinated data logging to ensure accuracy and reproducibility.

Figure 4.2 presents the on-site configuration. Using a custom-designed mounting system, the tri-axial accelerometer (Figure 4.2a) was embedded up to 1 meter from the pavement edge. It was aligned with the principal motion axes as follows:

- X-axis (Lateral, L): Perpendicular to the road edge
- Y-axis (Axial, A): Parallel to the traffic flow (longitudinal)
- Z-axis (Vertical, V): Perpendicular to the pavement surface (upward)

Nearby, the handheld LIDAR speed gun and Wi-Fi camera were manually operated to capture vehicle speed and visual traffic characteristics. As shown in Figure 4.2b, one team member recorded speed measurements using the LIDAR gun, while another documented vehicle type and axle configuration. This dual-recording ensured accurate synchronization of vibration data with ground truth traffic attributes.

A three-member research team coordinated the setup: one operator managed the vibration logging equipment, while two others handled visual observation and speed capture. This structured arrangement minimized external interference and ensured high-quality, temporally aligned data collection for each vehicle event.

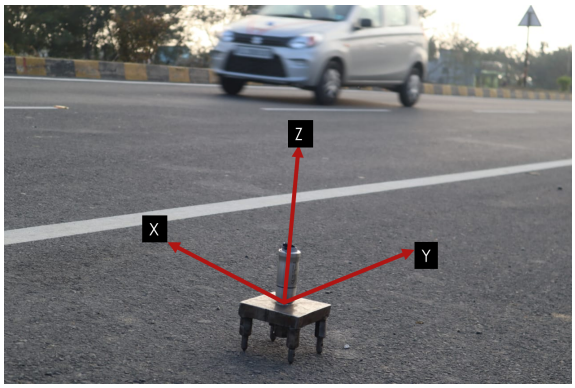

(a) Accelerometer mounted on pavement using custom mounting device

(b) Manual LIDAR speed measurement and vehicle annotation

Fig. 4.2 On-site deployment setup: vibration sensing and collaborative vehicle monitoring

4.3 Study Locations

This section presents the geographic and contextual settings of all field studies carried out as part of this research. While some studies shared common locations, others involved entirely separate sites due to different research objectives. Site-specific conditions, including road geometry, traffic environment and instrument deployment feasibility, played a crucial role in the site selection process. The following subsections describe the locations used in each study domain.

4.3.1 Vehicle Classification and Vibration Equivalence Studies

Figure 4.3 provides the layout of the selected sites used for the vehicle classification and RVEL/PCVE studies, conducted in Gorakhpur, a major city in the Purvanchal region of Uttar Pradesh, India. A comprehensive survey was undertaken to identify four optimal sites along highways outside the city center. These locations were specifically chosen for their flat, open layouts free of nearby buildings, parked vehicles, or other vibration-reflecting structures within a 60.8 m radius. The line of sight was clear within an arc of 120° and background vibrations were minimal. Each site was visually inspected to confirm pavement integrity, absence of potholes and accessibility for instrument setup. These efforts ensured that the collected data would be both reliable and consistent.

4.3.2 Route Optimization Study

Figure 4.4 illustrates the mapped locations used for the route optimization framework, which involved a large-scale survey conducted in two major Indian cities: Gorakhpur and Varanasi. A total of 52 mid-block sites were identified, 24 in Gorakhpur and 28 in Varanasi, along primary road corridors to ensure representative data capture. The local site selection prioritized two-lane roads where uninterrupted vehicle flow could be observed. Sites were

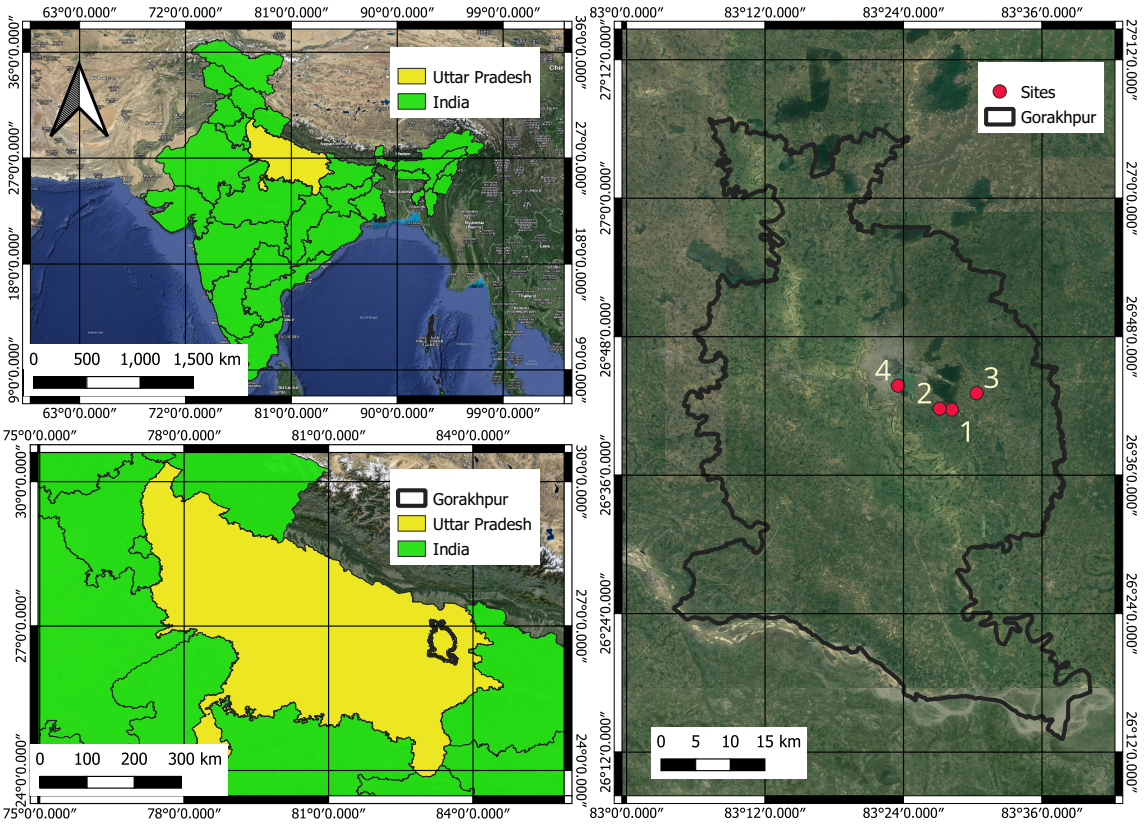

Fig. 4.3 Site layout and locations used for vehicle classification and RVEL/PCVE Study

positioned to reflect typical daily traffic variations during morning peak, evening peak and off-peak hours. Site-specific surveys determined peak periods based on market operations, school timings and public transport availability. The video camera was positioned at an elevated angle to capture both lanes. The geometric uniformity of selected roads supported consistent modeling assumptions.

4.3.3 Speed Hump Vibration Study

Figure 4.5 illustrates the data collection locations for the speed hump study, conducted at three distinct sites in Varanasi. Each location focused on a different hump profile: Fiber, Bitumen and Rumble Strips. The Fiber and Bitumen breakers were situated within the Banaras Hindu University (BHU) campus, while the Rumble Strip site was located on

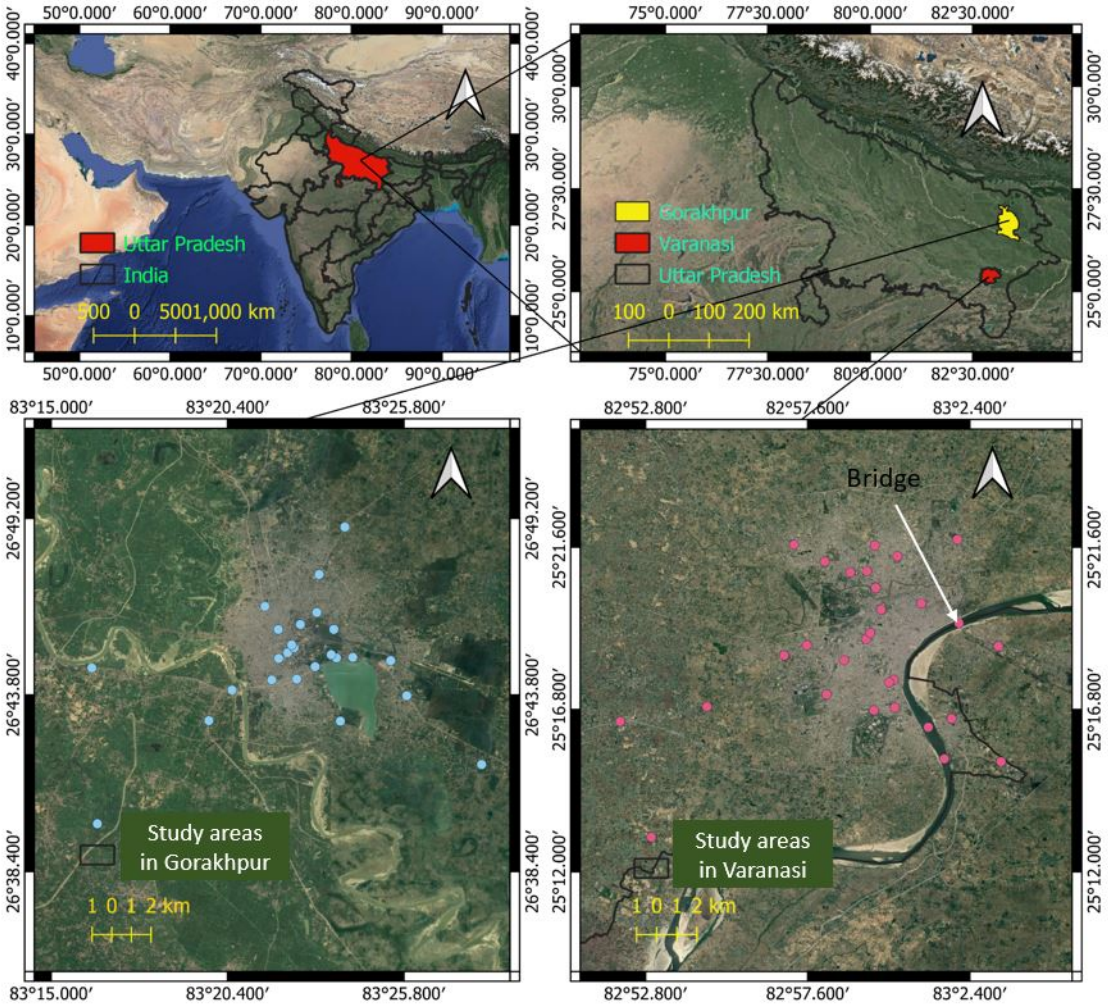

Fig. 4.4 An illustration of data collection sites in Varanasi and Gorakhpur, where dots in the water bodies indicate the bridges.

National Highway 2, adjacent to BHU. Sites were selected based on pavement uniformity, operational safety and suitability for sensor installation.

Each hump type was chosen to represent a common urban speed regulation strategy. These configurations facilitated the accurate capture of vehicle-induced vibrations under varying geometric discontinuities. Importantly, all the speed breakers assessed in this study were situated on bituminous flexible pavements, ensuring uniformity in the underlying surface material and its mechanical interaction with the vehicles. This consistent pavement condition minimizes confounding effects from surface rigidity or material heterogeneity,

allowing the study to isolate the influence of hump geometry itself. The geometric specifications of the speed humps are summarized in Table 4.1.

Table 4.1 Speed Hump Dimensions and Site Information

Site No.	Breaker Type	Height (m)	Width (m)	H/W Ratio	Location
1	Fiber	0.05	0.44	0.114	BHU Campus
2	Bitumen	0.13	2.05	0.063	BHU Campus
3	Rumble Strips	0.012	0.15	0.080	NH-2, near BHU

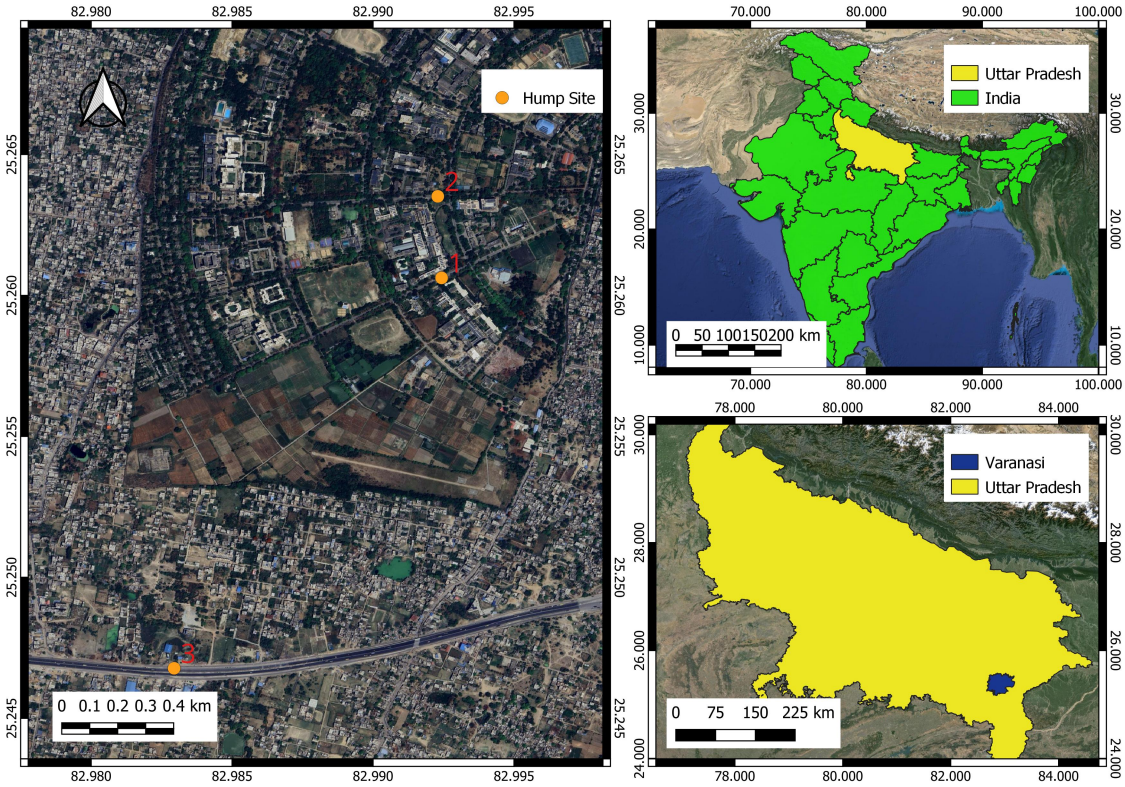

Fig. 4.5 Data collection locations

4.4 Signal Preprocessing Pipeline

This section outlines the unified signal preprocessing framework (Section 3.2) applied across all study domains to ensure consistency and comparability of vibration data. The preprocessing pipeline was carefully designed to transform the raw acceleration signals,

often noisy, baseline-shifted and inconsistent in length, into standardized, analyzable forms suitable for further segmentation and feature extraction. The overall workflow is illustrated in Figure 4.6.

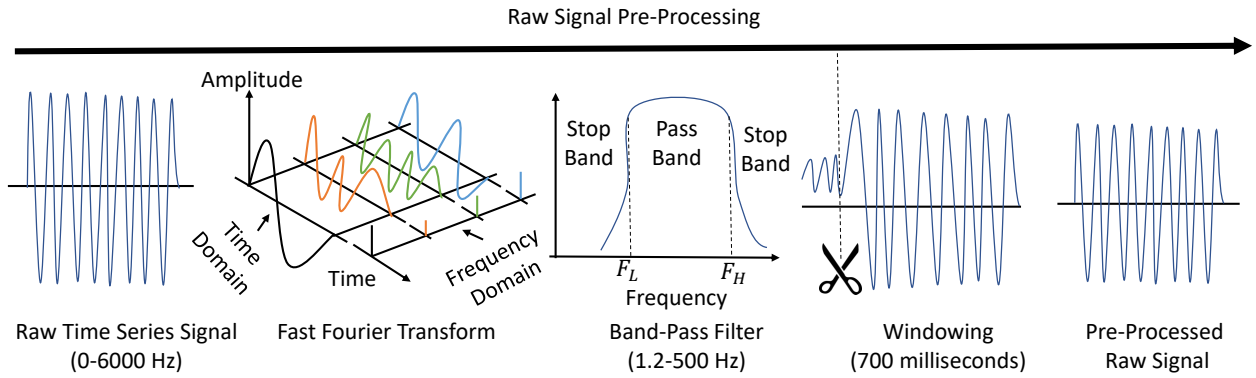

Fig. 4.6 Flow diagram of vibration signal dataset pre-processing.

4.4.1 Raw Signal Characteristics and Challenges

The raw signals in the collected dataset exhibit noise that must be removed for further processing. An example of such a signal is shown in Figure 4.7. The observed noise primarily arises from two sources: the DC offset introduced by the sensing instrument and background vibrations transmitted through the road pavement. Due to the presence of a DC component, the signal does not oscillate symmetrically around the zero baseline; instead, it is shifted upward, which distorts its statistical characteristics and spectral content. Effective preprocessing is therefore essential to restore signal fidelity and enable reliable feature extraction.

4.4.2 Spectral Insights Using FFT

A spectral decomposition was first conducted using Fast Fourier Transform (FFT) to guide the filter design and eliminate noise. This allowed the identification of both valuable and

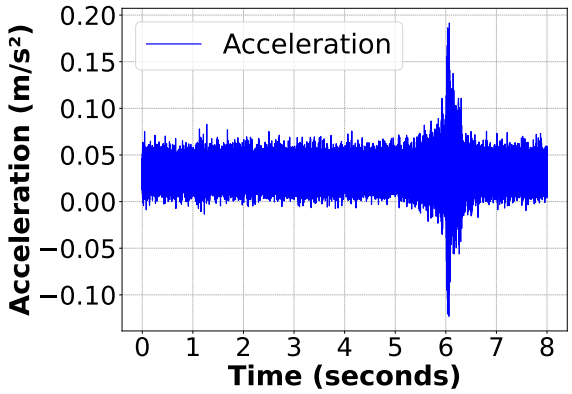

Fig. 4.7 Example of raw time-domain accelerometer signal (before preprocessing), showing baseline drift and noise.

unwanted frequency components. Figure 4.8 displays the FFT plots across two bands: the full bandwidth (0 to 6000 Hz) and a narrower focused band (1.2 to 500 Hz). These figures revealed that the most meaningful vibration content was concentrated below 500 Hz, while components above this threshold were primarily attributed to mechanical resonance and environmental noise.

The sampling frequency used in this study was 12,800 Hz, giving a Nyquist frequency of 6400 Hz. Hence, the frequency axis spans up to 6400 Hz. Visual inspection across multiple vehicle categories (e.g., truck, bus, LCV, car) consistently showed that vibration amplitudes rapidly decayed after approximately 480-520 Hz, while the dominant energy peaks lay within 50-400 Hz. This reinforced the selection of a 500 Hz upper cutoff.

4.4.3 Band-Pass Filtering: Justification and Application

Based on the FFT insights, a second-order Butterworth band-pass filter was applied with 1.2 Hz and 500 Hz cutoff frequencies. The lower limit (1.2 Hz) removed near-DC drift and environmental fluctuations (e.g., wind, power line interference) [64], while the upper limit suppressed high-frequency noise. For example, in a typical truck signal sampled at 12,800

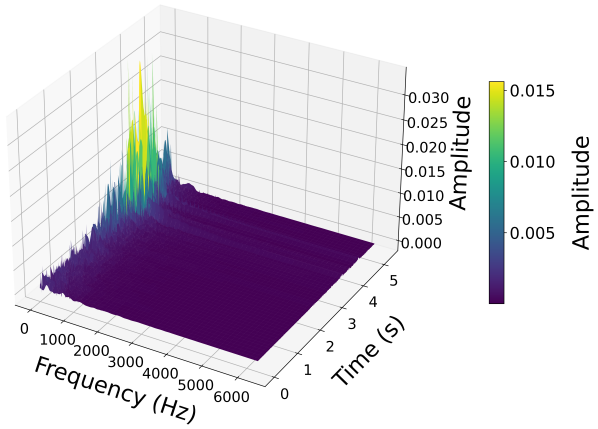

(a) FFT: 0-6000 Hz

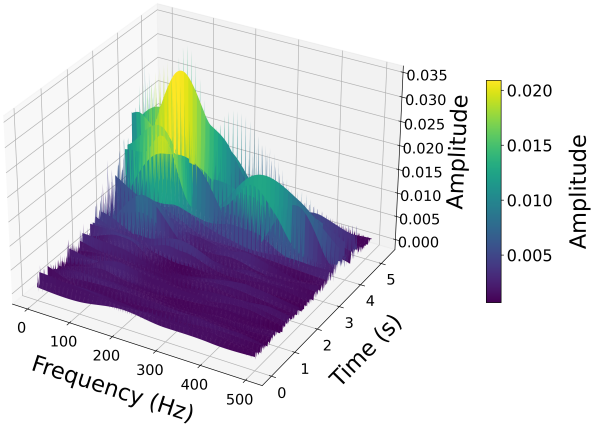

(b) FFT: 1.2-500 Hz

Fig. 4.8 FFT analysis of raw signal across broad and focused frequency bands.

Hz, the unwanted spectral spikes beyond 500 Hz were found to be less than 2% of the total energy, justifying their exclusion.

The Butterworth filter was chosen for its maximally flat frequency response in the passband and low phase distortion, preserving the integrity of transient features critical for downstream analysis. Figure 4.9 presents the filtered output, where the primary oscillatory content induced by vehicle-road interaction is retained, while high-frequency noise is effectively attenuated.

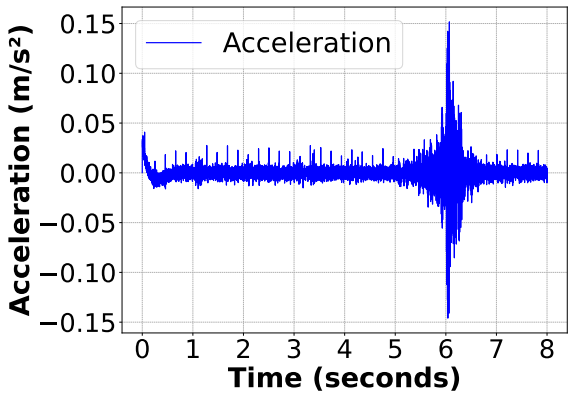

Fig. 4.9 Band-pass filtered signal retaining 1.2-500 Hz components.

The frequency response of the designed Butterworth filter is shown in Fig. 4.10, which illustrates the near-flat 0 dB gain within the 1.2-500 Hz passband and sharp attenuation beyond, validating both the cutoff choices and effective noise suppression.

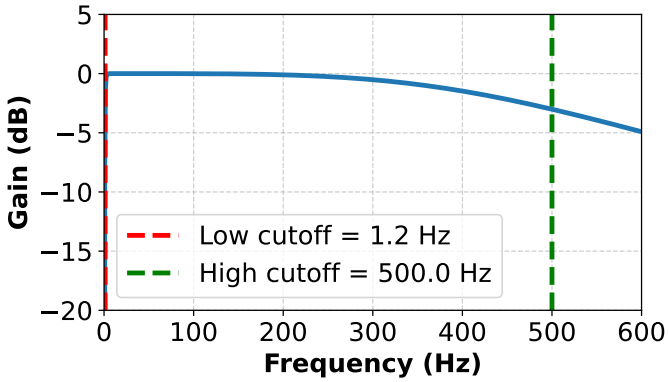

Fig. 4.10 Frequency response of the applied second-order Butterworth band-pass filter (1.2-500 Hz).

In addition to the FFT-based justification and the filter transfer function, the study computed 5%-damped pseudo-acceleration response spectra (PSA) from the experimental vibration time histories. These spectra were evaluated as functions of both frequency (0.5-1000 Hz) and period to capture the response trends across a wide dynamic range (Figures 4.11a and 4.11b). The results indicate that the measured vehicle-induced excitations generate the largest single-degree-of-freedom (SDOF) responses within the frequency band retained by the 1.2-500 Hz filter, whereas responses outside this band remain strongly

attenuated. This observation provides experimental support for the chosen passband and establishes a direct connection between the recorded ground vibrations and the structural response characteristics of interest.

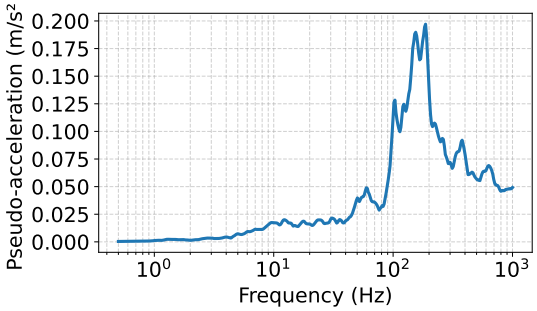

(a) PSA (5% damping) vs. frequency (0.5-1000 Hz).

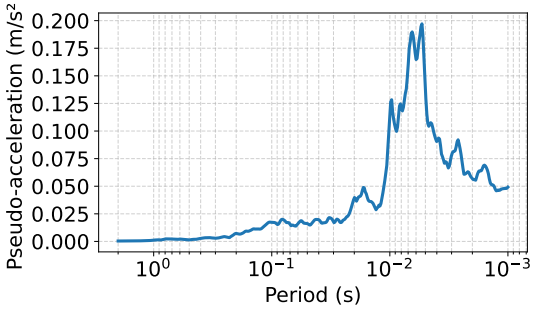

(b) PSA (5% damping) vs. period (log scale; short periods to the right).

Fig. 4.11 Experimental response spectra computed from measured ground-acceleration records.

Table 4.2 summarizes the empirical speed-frequency relationship derived from the median dominant frequencies across X, Y, and Z vibration directions for each vehicle class and speed bin. The results confirm that dominant frequencies increase with speed, with the Z-direction showing the strongest response due to vertical axle-pavement interaction, while X and Y capture lateral and longitudinal effects with class-specific variations. These findings validate that the measured vibration energy lies within the 1.2-500 Hz band and support the spectra illustrated in Figure 4.11.

Table 4.2 Empirical speed-frequency relationship (median dominant frequency in Hz) across vehicle classes and directions.

Direction	Vehicle Type	0-20	20-40	40-60	60-80	80-100	100-120
X	2-W	-	132.75	128.0	115.0	127.0	-
X	3-W	-	135.00	141.25	79.25	-	-
X	Bus	-	163.50	141.5	143.5	143.0	143.0
X	E-R	126.75	108.00	-	-	-	-
X	LCV	-	142.00	135.0	141.5	150.0	44.0
X	SUV	-	25.00	142.5	141.5	141.5	134.5
X	Tractor	136.0	139.00	116.5	-	-	-
X	Truck (ma)	-	147.00	144.5	146.25	154.75	-
X	Truck (s)	-	147.00	144.5	140.0	151.5	-
X	Truck (ta)	-	150.50	145.0	145.5	154.5	135.0
X	Truck (tr)	-	147.00	145.0	142.5	152.0	-
Y	2-W	-	140.25	138.5	131.5	136.5	-
Y	3-W	-	138.00	139.25	127.0	-	-
Y	Bus	-	136.50	139.5	140.0	141.5	144.0
Y	E-R	170.75	208.75	-	-	-	-
Y	LCV	-	133.00	140.0	144.5	148.5	118.5
Y	SUV	-	118.00	145.5	148.5	147.0	147.5
Y	Tractor	149.5	140.50	116.5	-	-	-
Y	Truck (ma)	-	150.00	144.5	139.0	136.5	-
Y	Truck (s)	-	145.25	146.0	137.5	132.5	-
Y	Truck (ta)	-	150.00	145.5	138.0	152.0	146.0

Continued on next page

Direction	Vehicle Type	0-20	20-40	40-60	60-80	80-100	100-120
Y	Truck (tr)	-	151.50	146.5	144.0	168.5	-
Z	2-W	-	31.50	32.0	31.0	30.0	-
Z	3-W	-	37.00	38.25	30.25	-	-
Z	Bus	-	31.50	26.0	27.0	26.5	18.5
Z	E-R	182.75	208.50	-	-	-	-
Z	LCV	-	27.50	29.5	30.5	34.0	43.5
Z	SUV	-	44.50	30.0	29.0	31.5	41.5
Z	Tractor	38.5	73.25	111.0	-	-	-
Z	Truck (ma)	-	28.50	28.5	29.5	27.0	-
Z	Truck (s)	-	24.00	26.5	27.5	27.5	-
Z	Truck (ta)	-	28.50	26.5	27.0	26.25	20.5
Z	Truck (tr)	-	30.00	29.0	26.5	24.0	-

4.4.4 Windowing and Removal of Transients

While filtering enhances spectral clarity, it can introduce edge artifacts, particularly at the start of the signal, due to filter-induced transients and early-stage noise, as shown in Figure 4.9 (at the start of the signal). To mitigate this, a fixed-duration segment of 700 milliseconds was removed from the beginning of each filtered signal.

Field observations guided this decision: the data acquisition system was typically triggered slightly before the vehicle fully entered the sensing zone. Consequently, the first 700 ms often contained partial approach dynamics or pre-event noise. At a sampling rate of 12,800 Hz, this corresponds to:

$$8960 = 0.7 \times 12800 \quad \text{samples},$$

Ensuring that the retained portion begins when the full vehicle-induced excitation is captured. This preprocessing step standardizes the start time across all samples, improving temporal alignment for downstream segmentation and analysis. Figure 4.12 illustrates the final windowed signal, now cleaned of initial transients and ready for subsequent processing.

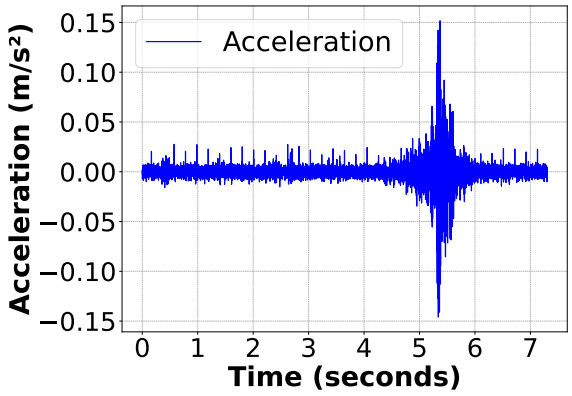

Fig. 4.12 Final signal after applying a rectangular window to remove initial transients.

Summary

The preprocessing pipeline comprising FFT-based spectral evaluation, second-order Butterworth filtering (1.2-500 Hz) and a calculated 700 ms window truncation eliminated drift, interference and start-of-recording distortions. These steps are tailored to this study's signal characteristics and acquisition protocol, forming a consistent base for further segmentation and feature extraction as detailed in the next section.

Windowing Strategy and FFT Conventions

0.7 s removal vs. 1 s analysis window: The 0.7 s duration corresponds to the initial transient portion discarded at the start of each recording (8960 samples at $f_s = 12{,}800$ Hz). This ensures that only the stable portion of the vehicle-induced vibration is retained. Subsequently, a fixed 1.0 s window (12,800 samples) is applied for segmentation and

feature extraction. Thus, the 0.7 s and 1 s durations represent two distinct stages: transient removal and standardized analysis windowing, respectively.

FFT notation. To avoid ambiguity, the following conventions are adopted:

- N: number of samples in the selected time-domain window (here $N = 12{,}800$ for 1 s).
- N_{FFT}: FFT length used for spectral estimation. In theory, the radix-2 FFT requires $N_{\text{FFT}} = 2^p \geq N$ (nearest power of two). In practice, the dBFA software employed in this study uses mixed-radix FFT algorithms with zero-padding, internally managing the FFT length while ensuring that the effective resolution is consistent with a power-of-two FFT.
- $N_{\max}$: symbol for maximum counts in other contexts, not related to FFT length.

Spectral resolution: With $f_s = 12{,}800$ Hz and software-selected FFT parameters, the resulting frequency resolution was $\Delta f \approx 0.625$ Hz (as reported by dBFA for a 500 Hz band divided into 801 lines). This value is consistent with standard FFT resolution expressions $\Delta f = f_s/N_{\text{FFT}}$, confirming equivalence between the theoretical radix-2 formulation and the software's implementation.

4.4.5 Signal Segmentation Using Maximum Energy Windowing

After preprocessing and transient removal, the next critical step involves segmenting the signal to isolate the portion that carries the most significant vibration response due to a vehicle pass-by. Given the non-uniform length of signals after 700 ms truncation, a fixed-duration segmentation strategy was adopted to ensure analytical consistency.

A fixed window size of 1 second, corresponding to 12,800 samples (given a sampling rate of 12,800 Hz), was used to segment the signal. This duration captures both transient

and steady-state dynamics of vehicle-induced vibrations. A fully overlapping sliding window approach was adopted with a stride of one sample to preserve signal continuity and ensure no localized peaks are missed.

Thus, each window begins exactly one sample after the previous one, resulting in maximal overlap and dense temporal coverage. The k^{th} window is defined as:

$$x_k = x[k : k + 12799], \quad \text{for } k = 0, 1, 2, \ldots, N - 12800,$$

Where N is the total number of samples in the filtered signal.

This approach ensures high-resolution segmentation suitable for capturing fine-grained temporal features essential for downstream machine learning tasks.

For every window, the energy was computed to assess the signal strength:

$$E_k = \sum_{n=0}^{12799} x_k(n)^2,$$

where $x_k(n)$ represents the n-th sample in the k-th window. The segment with the maximum energy, $k_{\max}$, was selected:

$$k_{\max} = \arg\max_k E_k,$$

and the corresponding window $x_{k_{\max}}$ was extracted as the final segment for further analysis.

This process ensures the retention of the signal region most influenced by the vehicle, eliminating quieter or trailing sections. The effectiveness of this segmentation can be observed in the figures below. Figure 4.13 highlights the maximum energy portion on a representative signal (Red segment) and Figure 4.14 shows the final 1-second segment extracted for analysis.

This uniform segmentation framework was applied across all signals in X, Y and Z directions, ensuring consistent feature extraction and comparability between different vehicle types and speed hump profiles.

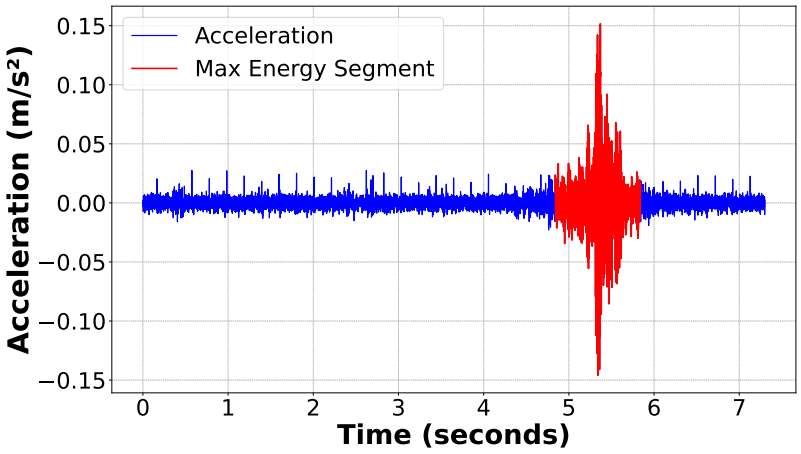

Fig. 4.13 Pre-processed signal with maximum energy window highlighted.

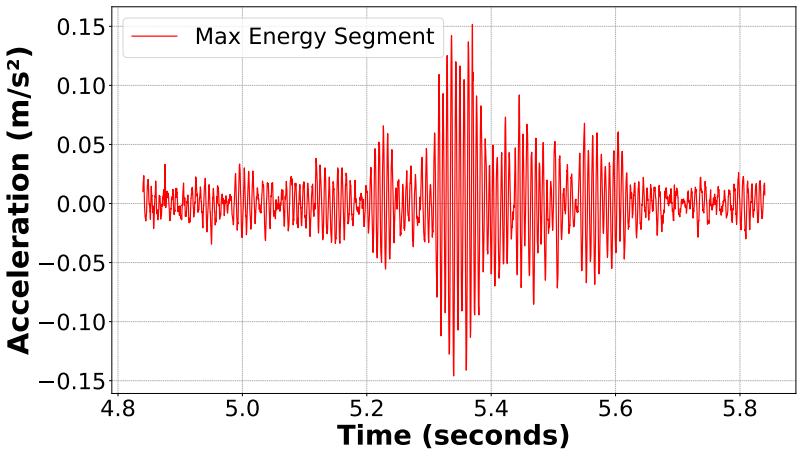

Fig. 4.14 Final extracted 1-second segment (12,800 samples).

4.5 Speed Hump Vibration Analysis

4.5.1 Introduction

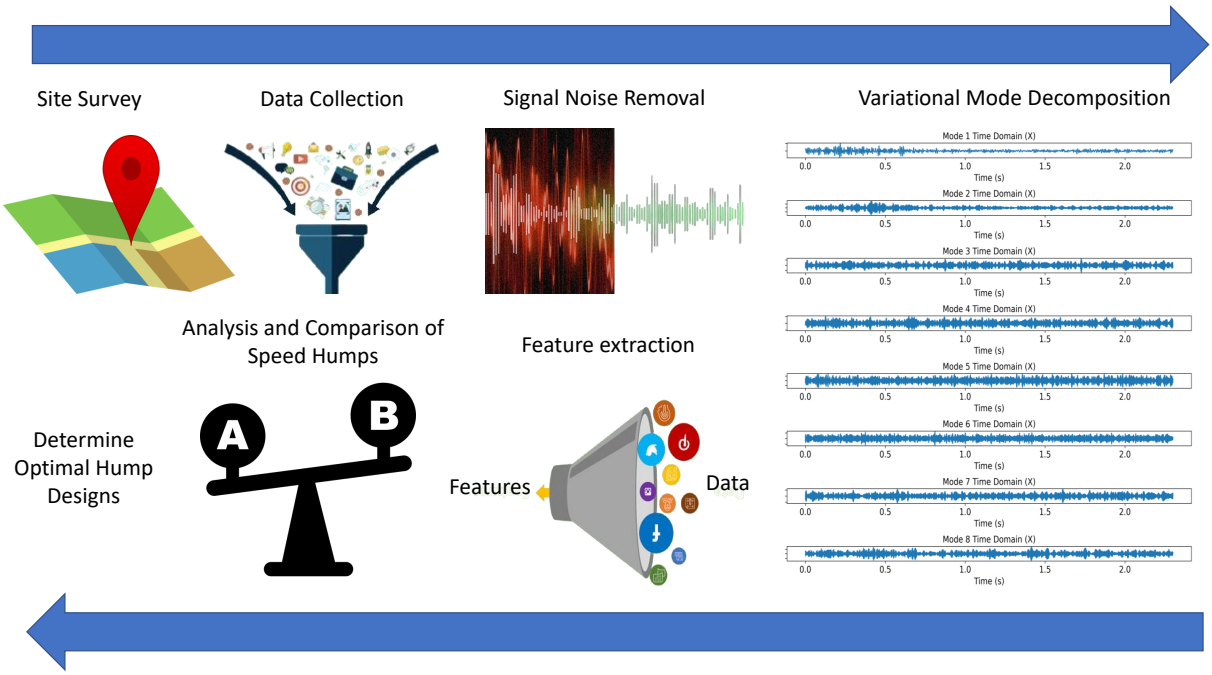

Fig. 4.15 Workflow of the proposed study on speed hump-induced vibrations.

This section outlines the methodology adopted specifically for the speed hump vibration study, as part of the broader research on traffic-induced vibrations. As the core instrumentation and signal preprocessing frameworks have been detailed in Sections 4.2 and 4.4, they are not repeated here. Instead, this section focuses on study-specific elements such as the objective, site selection rationale, dataset overview and vibration feature analysis.

The study workflow, as shown in Figure 4.15, comprises four integrated stages. First, representative sites were selected based on geometric diversity in speed hump profiles and feasibility of secure sensor deployment. Then, synchronized field instrumentation was established, including a tri-axial accelerometer for vibration acquisition, a LIDAR speed gun for velocity tracking and a Wi-Fi camera for visual vehicle classification.

Next, raw signals underwent preprocessing comprising FFT-based noise inspection, Butterworth band-pass filtering (1.2-500 Hz) and 700 ms transient removal. A fixed-length segment with maximum energy was isolated from the filtered signal for consistent comparison. The final analytical phase involved extracting two features: (1) global signal features such as RMS, maximum amplitude, energy and dominant frequency; and (2) VMD-based mode-specific features, including statistical descriptors and spectral metrics for each decomposed mode. This rigorous framework allowed for high-resolution investigation of dynamic vibration signatures due to varied hump geometries and vehicle classes.

4.5.2 Motivation and Objectives of This Study

Given the complexity and interdependence of factors such as hump geometry, material choice, vehicle dynamics, soil conditions and multi-directional vibrations, a holistic and integrated analysis approach is essential. This study aims to:

- Analyze vibrations in X, Y and Z directions across a wide range of vehicle types to evaluate real-world impacts comprehensively.

- Compare the vibrational effects of different speed humps materials like Fiber, Bitumen and Rumble Strips under varying speeds and load conditions.

- Employ advanced frequency-domain techniques, particularly Variational Mode Decomposition (VMD), to isolate and characterize dominant vibrational components for targeted mitigation.

- Integrate extensive field experiments, involving hundreds of vehicle pass-by events, with sophisticated signal processing methods to establish reliable and data-driven recommendations for speed hump designs.

4.5.3 Site Selection and Study Overview

Detailed site selection and hump dimension information is already presented in Section 4.3.3 and Table 4.1, along with Figure 4.5 illustrating data collection sites.

Three test sites in Varanasi were selected for their geometric uniformity and distinct hump profiles. All speed humps were located in operational roadways, ensuring realistic traffic flow. Data were recorded only during single-vehicle pass-by events. Figure 4.16 shows the sensor deployment at the data collection site.

Fig. 4.16 Illustrative layout of a speed hump profile and the associated sensor deployment.

4.5.4 Data Collection Overview

Tri-axial vibration data were collected using the instrumentation described in Section 4.2. The sensor was mounted 1 meter from the pavement edge using the custom anchoring mechanism. Only single-vehicle events were recorded to avoid overlapping responses. The study spanned 20 days and recorded 635 vehicle pass-by instances across nine vehicle categories.

Each vehicle was categorized manually using video footage and field observation. The categories include: 2-wheeler, 3-wheeler, car, bus, truck, LCV, e-rickshaw, battery

2-wheeler and tractor. The recorded vibration signals are expressed in terms of acceleration, with all values represented in (m/s^2) and the frequency in Hz.

4.5.5 Descriptive Dataset Summary

To provide clarity on the dataset used for vibration analysis, Tables 4.3, 4.4 and 4.5 summarize vehicle-wise descriptive statistics for each vibration axis X (lateral), Y (longitudinal) and Z (vertical). These tables present count, maximum amplitude, RMS, total energy and dominating frequency metrics. All acceleration-based metrics in these tables are reported in (m/s^2) and the frequency in Hz.

Table 4.3 Descriptive analysis of vehicle types across different breaker types for various X-axis metrics.

Breaker	**Vehicle**	**Count**	**X Max**				**X RMS**				**X Total Energy**				**X Dominating Freq**			
Type	**Type**		**Mean**	**Std**	**Min**	**Max**	**Mean**	**Std**	**Min**	**Max**	**Mean**	**Std**	**Min**	**Max**	**Mean**	**Std**	**Min**	**Max**
Bitumen	2-W	218	0.028	0.029	0.008	0.319	0.007	0.005	0.003	0.029	0.938	1.439	0.035	10.760	81	23	48	187
Bitumen	B 2-WB	20	0.016	0.003	0.013	0.018	0.004	0.001	0.003	0.006	0.271	0.137	0.114	0.419	85	14	68	101
Bitumen	3-W	15	0.041	0.021	0.016	0.097	0.011	0.004	0.004	0.018	1.718	1.259	0.197	4.062	79	14	53	100
Bitumen	Bus	12	0.181	-	0.181	0.181	0.058	-	0.058	0.058	42.910	-	42.910	42.910	78	-	78	78
Bitumen	Car	80	0.028	0.019	0.010	0.110	0.008	0.005	0.003	0.028	1.073	1.577	0.067	10.173	72	17	48	103
Bitumen	B 3-W	14	0.036	-	0.036	0.036	0.013	-	0.013	0.013	2.041	-	2.041	2.041	68	-	68	68
Bitumen	LCV	13	0.014	-	0.014	0.014	0.005	-	0.005	0.005	0.263	-	0.263	0.263	68	-	68	68
Bitumen	Tractor	19	0.025	-	0.025	0.025	0.008	-	0.008	0.008	0.823	-	0.823	0.823	55	-	55	55
Fiber	2-W	39	0.043	0.029	0.011	0.192	0.009	0.004	0.003	0.030	1.266	1.764	0.109	11.247	55	33	37	250
Fiber	3-W	18	0.026	-	0.026	0.026	0.007	-	0.007	0.007	0.578	-	0.578	0.578	42	-	42	42
Fiber	Car	16	0.042	0.019	0.013	0.070	0.010	0.005	0.003	0.020	1.429	1.383	0.151	5.022	43	8	36	70
Fiber	LCV	12	0.116	-	0.116	0.116	0.018	-	0.018	0.018	4.078	-	4.078	4.078	38	-	38	38
Rumble Strips	2-W	11	0.032	0.023	0.012	0.084	0.008	0.005	0.003	0.018	1.009	1.288	0.083	4.031	92	27	12	110
Rumble Strips	3-W	17	0.016	-	0.016	0.016	0.004	-	0.004	0.004	0.237	-	0.237	0.237	103	-	103	103
Rumble Strips	Bus	22	0.027	0.020	0.013	0.041	0.008	0.006	0.004	0.012	0.955	1.105	0.174	1.737	89	4	86	91
Rumble Strips	Car	13	0.029	0.017	0.011	0.059	0.008	0.005	0.003	0.019	1.200	1.440	0.131	4.650	106	50	46	264
Rumble Strips	LCV	10	0.023	0.008	0.013	0.036	0.006	0.002	0.004	0.008	0.463	0.239	0.188	0.862	119	64	73	274
Rumble Strips	Tractor	14	0.035	0.006	0.027	0.042	0.009	0.001	0.008	0.011	1.131	0.231	0.920	1.428	81	14	63	95
Rumble Strips	Truck	72	0.044	0.021	0.011	0.120	0.013	0.006	0.003	0.036	2.619	3.025	0.133	16.819	96	34	14	276

Table 4.4 Descriptive analysis of vehicle types across different breaker types for various Y-axis metrics.

Breaker	Vehicle	Count	Y Max				Y RMS				Y Total Energy				Y Dominating Freq			
Type	Type		Mean	Std	Min	Max	Mean	Std	Min	Max	Mean	Std	Min	Max	Mean	Std	Min	Max
Bitumen	2-W	218	0.025	0.016	0.010	0.126	0.007	0.004	0.003	0.022	0.730	0.936	0.037	6.093	81	40	24	187
Bitumen	B 2-WB	20	0.015	0.002	0.012	0.016	0.004	0.001	0.003	0.005	0.231	0.096	0.111	0.341	50	29	6	68
Bitumen	3-W	15	0.036	0.017	0.017	0.079	0.010	0.004	0.005	0.018	1.568	1.178	0.323	3.937	65	13	32	88
Bitumen	Bus	12	0.121	-	0.121	0.121	0.043	-	0.043	0.043	23.656	-	23.656	23.656	80	-	80	80
Bitumen	Car	80	0.026	0.015	0.011	0.083	0.007	0.004	0.003	0.020	0.850	1.023	0.091	5.017	66	19	31	167
Bitumen	B 3-W	14	0.041	-	0.041	0.041	0.014	-	0.014	0.014	2.363	-	2.363	2.363	68	-	68	68
Bitumen	LCV	13	0.016	-	0.016	0.016	0.005	-	0.005	0.005	0.300	-	0.300	0.300	70	-	70	70
Bitumen	Tractor	19	0.030	-	0.030	0.030	0.008	-	0.008	0.008	0.920	-	0.920	0.920	30	-	30	30
Fiber	2-W	39	0.046	0.031	0.012	0.139	0.009	0.004	0.003	0.020	1.189	1.216	0.112	5.190	49	10	16	72
Fiber	3-W	18	0.022	-	0.022	0.022	0.005	-	0.005	0.005	0.350	-	0.350	0.350	42	-	42	42
Fiber	Car	16	0.039	0.016	0.014	0.064	0.009	0.004	0.003	0.016	1.093	0.918	0.148	3.353	50	13	40	70
Fiber	LCV	12	0.064	-	0.064	0.064	0.017	-	0.017	0.017	3.652	-	3.652	3.652	70	-	70	70
Rumble Strips	2-W	11	0.028	0.021	0.012	0.084	0.007	0.004	0.003	0.015	0.841	1.038	0.098	3.044	95	23	30	119
Rumble Strips	3-W	17	0.014	-	0.014	0.014	0.004	-	0.004	0.004	0.177	-	0.177	0.177	61	-	61	61
Rumble Strips	Bus	22	0.026	0.017	0.014	0.039	0.007	0.004	0.004	0.010	0.695	0.735	0.176	1.215	100	14	90	110
Rumble Strips	Car	13	0.024	0.015	0.010	0.052	0.007	0.005	0.003	0.017	0.940	1.250	0.129	3.820	94	16	44	109
Rumble Strips	LCV	10	0.018	0.003	0.014	0.023	0.005	0.001	0.004	0.006	0.279	0.105	0.189	0.454	201	265	85	855
Rumble Strips	Tractor	14	0.024	0.003	0.021	0.027	0.007	0.001	0.006	0.008	0.606	0.133	0.516	0.801	86	7	76	92
Rumble Strips	Truck	72	0.037	0.020	0.010	0.110	0.011	0.006	0.003	0.040	2.110	3.045	0.118	20.930	100	18	19	142

Table 4.5 Descriptive analysis of vehicle types across different breaker types for various Z-axis metrics.

Breaker	Vehicle	Count	Z Max				Z RMS				Z Total Energy				Z Dominating Freq			
Type	Type		Mean	Std	Min	Max	Mean	Std	Min	Max	Mean	Std	Min	Max	Mean	Std	Min	Max
Bitumen	2-W	218	0.024	0.015	0.009	0.137	0.006	0.003	0.003	0.017	0.539	0.593	0.035	3.654	120	47	20	243
Bitumen	B 2-WB	20	0.012	0.001	0.011	0.014	0.003	0.000	0.003	0.004	0.156	0.039	0.130	0.215	115	34	73	151
Bitumen	3-W	15	0.031	0.021	0.014	0.097	0.006	0.003	0.004	0.013	0.614	0.539	0.218	2.311	116	53	28	179
Bitumen	Bus	12	0.034	-	0.034	0.034	0.010	-	0.010	0.010	1.179	-	1.179	1.179	78	-	78	78
Bitumen	Car	80	0.021	0.015	0.009	0.139	0.005	0.002	0.003	0.011	0.335	0.281	0.050	1.635	118	44	24	198
Bitumen	B 3-W	14	0.032	-	0.032	0.032	0.009	-	0.009	0.009	0.993	-	0.993	0.993	131	-	131	131
Bitumen	LCV	13	0.012	-	0.012	0.012	0.003	-	0.003	0.003	0.139	-	0.139	0.139	68	-	68	68
Bitumen	Tractor	19	0.049	-	0.049	0.049	0.015	-	0.015	0.015	2.761	-	2.761	2.761	178	-	178	178

Continued on next page

Table 4.5 continued from previous page

Breaker Type	Vehicle Type	Count	Z Max				Z RMS				Z Total Energy				Z Dominating Freq			
			Mean	Std	Min	Max	Mean	Std	Min	Max	Mean	Std	Min	Max	Mean	Std	Min	Max
Fiber	2-W	39	0.039	0.038	0.012	0.213	0.006	0.002	0.003	0.018	0.509	0.654	0.139	4.278	90	42	17	143
Fiber	3-W	18	0.034	-	0.034	0.034	0.004	-	0.004	0.004	0.182	-	0.182	0.182	53	-	53	53
Fiber	Car	16	0.035	0.013	0.014	0.053	0.006	0.003	0.004	0.012	0.575	0.501	0.167	1.947	69	52	17	140
Fiber	LCV	12	0.097	-	0.097	0.097	0.011	-	0.011	0.011	1.544	-	1.544	1.544	29	-	29	29
Rumble Strips	2-W	11	0.024	0.014	0.011	0.058	0.007	0.003	0.003	0.014	0.698	0.790	0.070	2.553	41	34	19	140
Rumble Strips	3-W	17	0.015	-	0.015	0.015	0.004	-	0.004	0.004	0.238	-	0.238	0.238	39	-	39	39
Rumble Strips	Bus	22	0.035	0.031	0.014	0.057	0.010	0.008	0.004	0.015	1.598	2.018	0.171	3.025	21	4	18	24
Rumble Strips	Car	13	0.025	0.017	0.011	0.063	0.007	0.005	0.003	0.020	0.921	1.421	0.123	5.207	46	46	14	173
Rumble Strips	LCV	10	0.022	0.006	0.014	0.033	0.005	0.001	0.004	0.008	0.395	0.183	0.183	0.778	61	66	16	198
Rumble Strips	Tractor	14	0.033	0.011	0.022	0.045	0.008	0.002	0.006	0.011	0.945	0.515	0.538	1.684	160	96	23	240
Rumble Strips	Truck	72	0.038	0.017	0.011	0.094	0.011	0.006	0.003	0.034	1.954	2.347	0.120	15.158	42	40	12	185

4.5.6 Signal Preprocessing and Feature Extraction

The unified signal preprocessing pipeline described in Section 4.4 was employed. After band-pass filtering (1.2-500 Hz) and windowing (removal of initial 700 ms), each signal was segmented based on maximum energy windowing. This ensured consistency across all vehicle classes.

Feature extraction followed a two-tiered approach:

- **Unified Signal Features:** Max, RMS, total energy and dominating frequency as summarized in Section 3.3.3.
- **VMD-Based Features:** For each mode obtained using Variational Mode Decomposition, time-domain (mean, RMS, skewness, kurtosis, etc.) and frequency-domain features (dominant frequency, PSD, SNR) were extracted (refer Section 3.3.2, Section 3.3.3).

This structured analysis provided a multi-resolution understanding of vehicle-hump interaction patterns.

4.6 Reference Vibration Emission Level (RVEL) and Passenger Car Vibration Equivalence (PCVE)

4.6.1 Introduction

This section presents the second major study, focusing on vibration emissions from vehicles traversing uninterrupted, flat roadway segments. Unlike the earlier analysis over speed humps (Section 4.5), this study quantifies generalized traffic-induced vibrations (TIV) under free-flow conditions, emphasizing benchmark emissions and vehicle-type normalization.

The analytical pipeline (Figure 4.17) includes site survey, tri-axial accelerometer and speed gun data collection, FFT-based spectral assessment, band-pass filtering (1.2-500 Hz) and windowing to extract peak-energy signal segments (see Sections 4.4.3 and 4.4.5). Key metrics, including maximum acceleration, RMS and average power, feed into the regression-based Reference Vibration Emission Level (RVEL) framework (Section 3.4), which models speed-vibration relationships by vehicle type and motion axis (X, Y, Z). These outputs enable the computation of Passenger Car Vibration Equivalence (PCVE), translating the vibration impact of various vehicles into passenger-car-equivalent units.

Finally, all models and computations are integrated into a software tool designed for planners, engineers and policymakers to assess TIV in real time or for transport infrastructure planning.

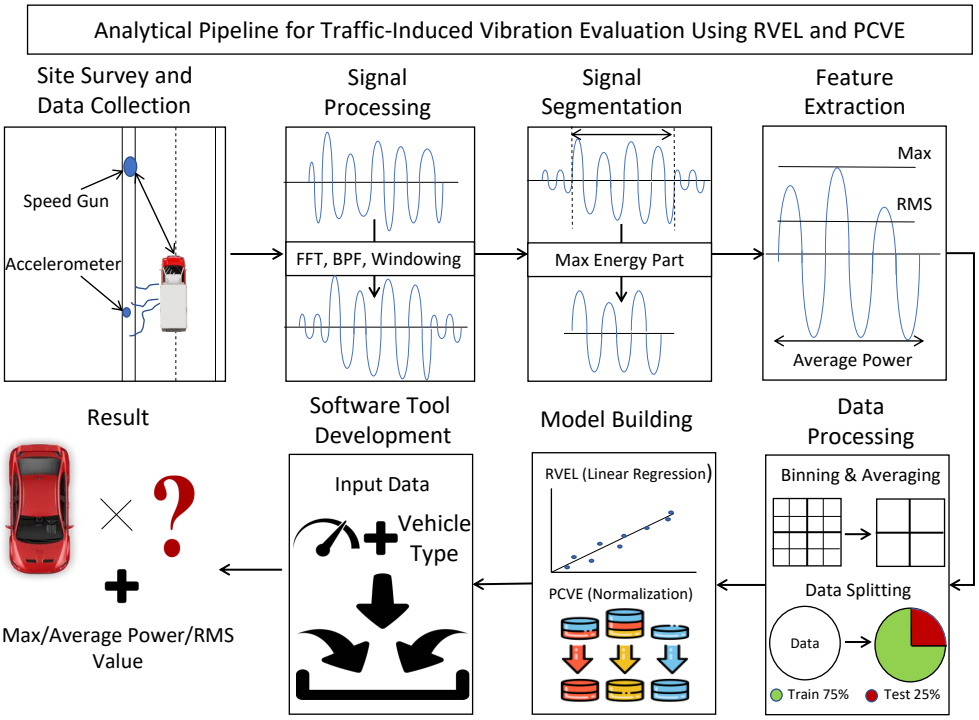

Fig. 4.17 Workflow of Traffic-Induced Vibration Analysis Using RVEL and PCVE

4.6.2 Motivation and Objectives

The motivation behind this study stems from the limitations of conventional vibration assessment standards that rely on generalized thresholds such as peak particle velocity (PPV) without accounting for vehicle-specific dynamics. In real-world traffic, diverse vehicle classes, including multi-axle trucks, light commercial vehicles and two-wheelers, exert fundamentally different vibration signatures on the pavement. These disparities are further influenced by axle configuration, gross weight and speed. The lack of a class-specific framework can lead to the underestimation or overestimation of vibrational risks, particularly in environments hosting sensitive structures such as heritage buildings, laboratories, or residential zones.

To bridge this gap, the study introduces two integrated frameworks: (i) the Reference Vibration Emission Level (RVEL) model, which establishes statistically validated vibration

baselines for each vehicle type; and (ii) the Passenger Car Vibration Equivalence (PCVE) metric, inspired by the PCU (Passenger Car Unit) concept used in traffic flow analysis, which standardizes vibration outputs across vehicle categories.

The primary objectives of this study are:

- To develop a comprehensive data-driven RVEL framework that quantifies the relationship between vehicle speed and vibrational intensity (across X, Y and Z axes) for each vehicle class using field measurements on flat road segments.
- To formulate the PCVE metric, enabling cross-category comparisons of vibration emission by expressing outputs in terms of passenger-car-equivalent units.
- To provide a generalized, scalable methodology that supports the integration of TIV evaluation into policy formulation, infrastructure planning and vibration-sensitive urban design.

Instrumentation and Data Logging

The instrumentation framework employed in this study aligns with the standardized setup already detailed in Section 4.2. Ground-borne vibrations in the lateral (X), longitudinal (Y) and vertical (Z) directions were measured using the tri-axial wireless accelerometer system (*01 dB, ACOEM, France*), mounted via the patent-pending custom baseplate (Section 4.2.2). Vehicle speeds were captured using the Stalker XS LIDAR gun (Section 4.2.3), while synchronized visual recordings facilitated vehicle identification (Section 4.2.4). All instruments were deployed according to the configuration illustrated in Figure 4.2, with data acquired during free-flow traffic conditions to avoid interference from acceleration, deceleration, or platooning effects.

The consistency in instrumentation across this and the earlier speed hump study (Section 4.5) ensured methodological coherence and comparability. Instrument placement,

directional alignment and event annotation protocols followed the validated procedures from earlier deployments.

Site Selection and Deployment

Site selection was conducted using the criteria outlined in Section 4.3.1, focusing on geometric uniformity, minimal environmental noise and unobstructed sensor placement (Section 4.2.5). The selected road segments in Gorakhpur, a key urban node in the Purvanchal region of India, were chosen to ensure isolation of vehicle-induced vibrations from extraneous sources. Each site was validated for surface integrity and absence of reflective structures within a 60.8 m radius. Figure 4.3 provides an overview of the selected locations.

Dataset Description

The field campaign resulted in a comprehensive dataset comprising 9,257 single-vehicle pass-by events. Each record includes the annotated vehicle type, instantaneous speed and tri-axial ground acceleration signals, measured in m/s². Data were acquired under uniform pavement and environmental conditions, enabled by a rigorous site selection strategy to minimize external variability.

The dataset captures the full spectrum of vehicle categories commonly encountered on Indian highways and urban roads, including: 2-wheelers (1,901), 3-wheelers (139), passenger cars (1,719), light commercial vehicles (LCVs, 520), buses (291), tractors with trolley (83), battery-operated e-rickshaws (283) and trucks with varying axle configurations, single axle (1,054), tandem axle (1,174), multi axle (1,063) and tridem axle (1,030). These classifications reflect the heterogeneous vehicle mix typical of Indian traffic systems.

Vehicle speeds ranged from 10 km/h (e-rickshaws) to 130 km/h (high-speed passenger cars), encompassing urban and highway operating regimes. Figure 4.18 visualizes the

distribution of vehicle classes, with trucks and two-wheelers emerging as the most frequent contributors, critical for assessing vibration loads in mixed-traffic environments.

Each data point consists of the vehicle's type, speed (in km/h) and associated tri-axial vibration signal, providing a rich foundation.

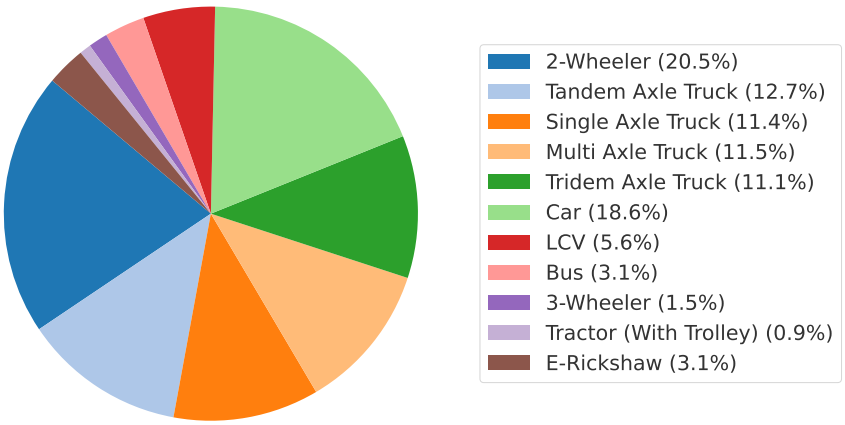

Fig. 4.18 Percentage distribution of vehicle types in the dataset.

4.6.3 Data Pre-Processing

The transition from raw vibration signals to uniform-length segmented signals was accomplished through a standardized pre-processing pipeline, as detailed in Sections 4.4. This pipeline included FFT-based noise identification, band-pass filtering and transient removal using windowing. The resulting clean signals were further segmented using an energy-based windowing approach to isolate the most informative portion of each signal corresponding to vehicle passage.

4.6.4 Feature Extraction from the Maximum Energy Segment

Key features are derived from the segment corresponding to the highest energy window $x_{k_{\max}}$ to characterize the signal effectively. These features include:

- **Maximum Amplitude:** The peak value within the window, calculated as $\max_n |x_{k_{\max}}(n)|$, provides insight into the signal's maximum intensity for acceleration, crucial for analyzing peak behavior. For the combined amplitude across the X, Y and Z directions, the root-sum-of-squares (RSS) method is used:

$$A_{\text{combined}} = \sqrt{A_X^2 + A_Y^2 + A_Z^2},$$

Where A_X, A_Y, A_Z are the maximum amplitudes in the X, Y and Z directions, respectively.

- **Root Mean Square (RMS):** A measure of the signal's overall power, given by

$$\text{RMS} = \sqrt{\frac{1}{12800} \sum_{n=0}^{12799} x_{k_{\max}}(n)^2},$$

Offers an average assessment of the signal's energy, making it robust against outliers. The combined RMS magnitude across the X, Y and Z directions is computed as:

$$\text{RMS}_{\text{combined}} = \sqrt{\text{RMS}_X^2 + \text{RMS}_Y^2 + \text{RMS}_Z^2},$$

Where $\text{RMS}_X, \text{RMS}_Y, \text{RMS}_Z$ are the RMS values for the X, Y and Z directions, respectively.

- **Total Energy:** The total energy in the segment is computed as

$$E_{\text{total}} = \sum_{n=0}^{12799} x_{k_{\max}}(n)^2 \quad \text{(unit: } \text{m}^2/\text{s}^4\text{)}.$$

- **Average Power:** The average power in the segment is calculated by normalizing the total energy with the sampling frequency and scaling to convert to microwatts (μW):

$$P_{\mu\text{W}} = E_{\text{total}} \times \frac{1}{12800} \times 10^6 \quad \text{(unit: } \mu\text{W)}.$$

For the combined average power across the X, Y and Z directions, a summation method is applied:

$$P_{\text{combined}} = P_X + P_Y + P_Z,$$

Where P_X, P_Y, P_Z are the average power values for the X, Y and Z directions, respectively.

The extraction of these features provides a detailed representation of the signal within the maximum energy window, offering valuable insights for subsequent analysis or classification tasks. Table 4.6 presents the descriptive statistics of the entire dataset, where the Max and RMS values are expressed in terms of acceleration (mm/s^2), speed is represented in kilometers per hour (km/h) and the Avg. Pow. (Average Power) of signal values is represented in units of (μW). Notably, multi-axle trucks (T(ma)) and tridem-axle trucks (T(tr)) exhibit significantly higher maximum accelerations and average power values across all axes compared to smaller vehicles such as two-wheelers (2-W) and three-wheelers (3-W). For instance, T(ma) vehicles demonstrate a mean vertical acceleration of 37.97 mm/s^2 and an average power of 87.86 μW, indicating their substantial vibrational impact. Additionally, buses (Bus) record the highest maximum accelerations in all directions, surpassing passenger cars (Car) and other truck categories. The standard deviations (std) reveal significant variability among heavy vehicle classes, suggesting diverse operational conditions and load distributions. Extreme values, such as a maximum average power of 430.92 μW for T(ma) vehicles, underscore the urgent need for targeted vibration mitigation strategies in high-impact vehicle categories. The abbreviations used in the table are as

follows: 2-W refers to a 2-Wheeler, 3-W to a 3-Wheeler, T(ta) to a Tandem Truck, T(s) to a Single Truck, T(ma) to a Multi-Axle Truck, T(tr) to a Tridem Axle Truck, TT to a Tractor with Trailer and E-R to a Battery-Operated Rickshaw.

Table 4.6 Descriptive Data for All Vehicles

Vehicle	Metric	X			Y			Z			Speed
		Max	RMS	Avg. Pow.	Max	RMS	Avg. Pow.	Max	RMS	Avg. Pow.	
2-W	mean	22.95	3.95	34.31	12.05	3.26	28.33	12.23	3.23	27.98	56.69
2-W	std	3.80	0.81	7.96	3.44	0.80	7.56	2.90	0.37	4.08	12.21
2-W	min	11.45	3.12	15.08	7.68	2.64	13.18	8.11	2.81	13.62	22.00
2-W	max	45.33	14.12	124.83	45.95	10.97	96.93	46.44	6.12	54.10	110.00
T(ta)	mean	31.70	7.40	65.43	21.34	5.76	50.87	21.30	5.41	47.80	50.49
T(ta)	std	13.61	4.06	35.93	11.36	3.22	28.48	9.33	1.90	16.80	8.47
T(ta)	min	14.65	3.11	15.06	8.76	2.76	13.37	10.04	2.98	15.90	29.00
T(ta)	max	132.34	32.96	291.34	85.90	24.21	213.99	95.24	17.11	151.22	102.00
T(s)	mean	26.07	5.45	48.07	16.42	4.31	37.98	19.07	4.81	42.38	52.98
T(s)	std	7.08	2.00	17.79	7.09	1.78	15.72	7.15	1.33	11.81	9.21
T(s)	min	14.80	3.32	16.09	8.51	2.81	14.14	10.05	3.01	15.96	29.00
T(s)	max	78.41	16.43	145.18	54.28	14.41	127.37	61.64	11.29	99.76	98.00
LCV	mean	23.98	4.49	39.26	13.83	3.62	31.71	15.92	3.92	34.29	62.51
LCV	std	5.56	1.33	11.91	6.44	1.29	11.59	10.23	1.27	11.30	12.59
LCV	min	12.59	3.15	15.27	8.54	2.63	12.73	8.46	2.94	14.25	28.00
LCV	max	68.12	14.60	129.02	81.14	16.88	149.18	156.88	19.22	169.86	126.00
Car	mean	23.53	4.20	36.17	13.13	3.41	29.29	12.78	3.35	28.76	79.07
Car	std	4.20	0.83	8.42	4.07	0.75	7.23	2.93	0.37	4.46	15.71
Car	min	10.91	3.10	15.00	7.71	2.67	12.94	8.09	2.84	13.77	11.00
Car	max	47.38	9.37	82.78	42.87	8.30	73.39	42.95	5.95	52.60	134.00
T(ma)	mean	37.97	9.95	87.86	27.69	7.86	69.41	23.73	6.24	55.12	47.61
T(ma)	std	18.86	6.07	53.69	17.03	5.36	47.44	11.93	2.55	22.64	7.47
T(ma)	min	15.09	3.14	15.20	9.57	2.78	13.46	10.26	3.05	14.77	26.00
T(ma)	max	170.04	48.75	430.92	123.22	44.35	392.05	138.80	24.56	217.09	84.00
T(tr)	mean	33.65	8.15	71.98	23.68	6.35	56.04	22.07	5.69	50.23	50.72

Continued on next page

Table 4.6 continued from previous page

Vehicle	Metric	X			Y			Z			Speed
		Max	RMS	Avg. Pow.	Max	RMS	Avg. Pow.	Max	RMS	Avg. Pow.	
T(tr)	std	15.18	4.36	38.59	12.76	3.49	30.88	9.61	1.95	17.31	7.89
T(tr)	min	13.20	3.33	16.10	8.83	2.83	14.38	10.20	3.03	14.67	28.00
T(tr)	max	136.02	33.14	292.95	98.69	28.75	254.13	89.21	17.32	153.08	97.00
Bus	mean	50.25	11.91	103.72	38.55	9.41	81.94	32.22	7.20	62.75	74.15
Bus	std	33.82	8.52	74.05	27.20	6.91	60.30	16.57	2.90	25.30	13.29
Bus	min	15.51	3.21	15.54	8.56	2.73	13.20	8.87	2.94	14.33	38.00
Bus	max	229.02	53.27	470.86	180.92	44.54	393.67	99.05	17.35	153.39	110.00
3-W	mean	22.45	4.18	36.46	12.46	3.33	28.93	14.16	3.67	31.98	42.89
3-W	std	4.07	0.60	6.36	3.01	0.48	4.97	3.70	0.54	5.59	7.48
3-W	min	12.08	3.31	16.21	9.06	2.80	14.02	9.17	3.01	14.63	26.00
3-W	max	35.27	6.05	53.49	25.65	5.20	45.99	33.32	5.70	50.38	63.00
TT	mean	47.56	13.35	118.01	34.51	10.17	89.91	24.32	6.32	55.88	30.01
TT	std	18.57	6.28	55.51	14.87	4.75	41.96	7.95	1.78	15.74	5.78
TT	min	20.38	4.53	40.08	11.68	3.08	27.20	11.52	3.57	31.53	20.00
TT	max	101.27	32.20	284.58	69.62	23.95	211.70	46.21	9.66	85.35	59.00
E-R	mean	25.79	5.41	47.64	17.73	5.15	45.38	14.50	3.84	33.83	15.60
E-R	std	4.36	1.44	13.01	8.04	2.76	24.52	3.33	0.64	5.92	3.64
E-R	min	14.58	3.31	16.37	8.65	2.71	13.99	8.79	2.89	13.97	7.00
E-R	max	42.27	10.96	96.91	49.74	16.30	144.03	28.86	6.77	59.81	27.00

Reference Vibration Emission Levels (RVEL) and Passenger Car Vibration Equivalence (PCVE)

This subsection outlines the integrated framework of Reference Vibration Emission Levels (RVEL) and Passenger Car Vibration Equivalence (PCVE) employed to model and assess traffic-induced vibrations (TIV) across various vehicle classes. The framework (Section 3.4) is based on a systematic, data-driven approach that utilizes the complete

dataset for model estimation. This full-data approach maximizes statistical power and enables robust inference regarding the relationship between vehicle speed and vibration metrics.

Data Binning and Averaging: To manage the extensive dataset comprising 9,257 single-vehicle pass-by events, a binning and averaging strategy was implemented, inspired by Wickham's *bin-summarise-smooth* framework [257]. This approach involved segmenting vehicle speeds (S) into discrete intervals (bins) and computing the average vibration metrics within each bin. The key steps are as follows:

1. **Sorting and Windowing:** The dataset was sorted based on vehicle speed ('kmph'). A sliding window technique with varying window sizes (e.g., 5 km/h) was applied to create speed bins.

2. **Averaging Metrics:** For each speed bin, vibration metrics like Maximum Amplitude (A_D), Root Mean Square (RMS_D) and Average Power (E_D) were averaged to obtain representative values for that interval.

3. **Unit Conversion:** Acceleration metrics were converted from m/s^2 to mm/s^2 and energy metrics were converted to μW to ensure consistency across measurements.

4. **Data Filtering:** Bins with fewer than five averaged samples were excluded to enhance the reliability of subsequent regression models.

This methodology effectively reduces data complexity, mitigates the impact of outliers and ensures that the regression analyses are based on robust and representative data points.

The splitting was performed using a random sampling method to ensure that each vehicle class is adequately represented in both subsets, minimizing bias and enhancing the model's predictive capability.

Model Building: Reference Vibration Emission Levels (RVEL): The RVEL framework aims to establish baseline vibration metrics for each vehicle class by quantifying the relationship between vehicle speed and vibration intensity across three orthogonal directions: longitudinal (X), lateral (Y) and vertical (Z).

Linear Regression Models: For each vehicle class C and vibration direction $D \in \{X, Y, Z\}$, a linear regression model was formulated as:

$$V_{D,C} = \alpha_{D,C} \cdot S + \beta_{D,C} + \varepsilon_{D,C} \tag{4.1}$$

Where: $V_{D,C}$ represents the vibration metric (Max, RMS, or Avg. Power) in direction D for a specific vehicle class C. The variable S denotes the vehicle speed in km/h. The parameter $\alpha_{D,C}$ is the slope, indicating the change in the vibration metric per unit speed, while $\beta_{D,C}$ is the intercept, representing the baseline vibration metric at zero speed. Finally, $\varepsilon_{D,C}$ is the error term, accounting for variability not explained by the model.

Physical basis and units: RVEL represents the baseline vibration emission of a vehicle class as a function of speed and axis, and it is grounded in dynamic tire-pavement-soil interaction. Heavier axle loads and higher speeds increase contact force fluctuations, which excite pavement-soil impedance and produce measurable ground accelerations. Since $V_{D,C}$ is defined in terms of physical vibration metrics, **RVEL is dimensional** and inherits the units of the chosen metric: mm/s^2 for Max and RMS acceleration, and μW for Average Power. The studied content band of 1.2 to 500 Hz captures suspension, body, and tire-related modes under free-flow operation, consistent with the preprocessing in Section 4.6.4.

Rationale for Linear Regression: The selection of simple linear regression for RVEL modeling is justified by its balance between simplicity and effectiveness. This

approach establishes a clear and interpretable relationship between vehicle speed and vibration metrics, which is fundamental for defining Reference Vibration Emission Levels (RVEL) across various vehicle classes. Linear regression is computationally efficient and adept at capturing the predominantly proportional relationship observed in the data. In addition, the method supports robust statistical inference through t-tests for individual coefficient significance and F-tests for overall model validation, making it well-suited for the intended application.

Engineering utility of RVEL: RVEL provides absolute, speed-dependent baselines by vehicle class and axis. These baselines support thresholding and auditing against planning criteria, screening of corridors with heavy vehicle proportions, and sensitivity analyses for speed regulation and lane assignment. Where lack of fit is detected, the same workflow can be extended to non-linear forms without changing the interpretability of $V_{D,C}(S)$ as an absolute emission reference.

Model Training and Validation: In the present study, regression models were developed using the entire dataset to maximize statistical power and achieve precise estimation of the model parameters ($\alpha_{D,C}$ and $\beta_{D,C}$). For each vehicle class and vibration metric, the least squares method was employed to derive the corresponding parameters. The performance of these models was evaluated using key metrics such as the coefficient of determination (R^2), Root Mean Square Error (RMSE) and Relative Mean Error (RME). Moreover, the statistical significance of individual regression coefficients was assessed via t-tests, while the overall model significance was examined using the F-test. This methodological framework ensures that the relationship between vehicle speed and vibration intensity is modeled statistically robustly and predictably.

Passenger Car Vibration Equivalence (PCVE): The *Passenger Car Vibration Equivalence* (PCVE) framework extends the concept of Reference Vibration Emission Levels (RVEL) by expressing vehicle-induced vibration metrics in terms of "passenger-car-equivalent" units, analogous to the Passenger Car Unit (PCU) concept used in traffic flow analysis. This approach allows different vehicle classes (e.g., buses, trucks, or motorcycles) to be converted into a standard reference scale based on passenger cars, enabling consistent comparisons and regulatory assessments of vibration impacts.

Derivation of PCVE from RVEL: PCVE values are obtained by first using the RVEL regression models for each vehicle class to predict vibration metrics ($V_{D,C}(S)$) at various speeds (S). These predicted values are then normalized against the corresponding vibration metrics for the passenger car class (C_{Car}), ensuring that all vehicles are measured relative to a standardized passenger car baseline:

$$\text{PCVE}_{D,C}(S) = \frac{V_{D,C}(S)}{V_{D,C_{\text{Car}}}(S)} \tag{4.2}$$

This normalization process enables direct comparisons of vibrational impacts across multiple vehicle types by framing each vehicle's vibration contribution in "passenger-car units." By capturing variations in dynamic load characteristics (e.g., axle configurations and speeds), the PCVE framework facilitates the development of targeted mitigation strategies. It informs decisions regarding infrastructure planning, traffic management and protecting sensitive structures.

Table 4.7 Dimensionality and units for vibration metrics and indices in the RVEL-PCVE framework.

Quantity	Dimensionality	Units
Max acceleration V (per axis)	Dimensional	mm/s^2
RMS acceleration V (per axis)	Dimensional	mm/s^2
Average Power V (per axis)	Dimensional	μW
RVEL $= V_{D,C}(S)$	Dimensional	Same as V
PCVE	Non dimensional	–

ISO 2631-1 and BS 6472 provide generalized guidance for human exposure and building vibration. The proposed RVEL-PCVE indices are designed to complement these documents by offering data-driven, vehicle-specific baselines and relative equivalence for site-specific interpretation.

Implementation in Software Tool: A custom Python-based software tool was developed to operationalize the RVEL-PCVE framework. This tool integrates the regression models derived from the binned and averaged data, enabling users to input vehicle speed values and obtain corresponding RVEL and PCVE predictions. The software features an intuitive graphical user interface (GUI) built with PyQt5, allowing seamless selection of vehicle types, metrics and vibration directions. Real-time visualizations of regression equations and predictions are facilitated through integrated matplotlib plots, enhancing user interaction and data interpretation. By reading regression parameters from an external configuration file, the software ensures flexibility and ease of updates, making the RVEL-PCVE framework accessible to stakeholders involved in infrastructure planning, traffic management and policy development.

The algorithm1 presents a structured approach to model and validate traffic-induced vibration (TIV) data using regression-based Vibration Energy Levels (RVEL) and Passenger

Car Vibration Equivalence (PCVE). It includes data pre-processing, binned averaging, model training, validation and a software tool for prediction and visualization. Below is the step-by-step outline:

4.7 Vehicle Classification Study

4.7.1 Introduction

This study proposes a vibration-based framework for vehicle classification using tri-axial accelerometer data recorded during single-vehicle pass-by events. The methodology integrates advanced signal pre-processing, energy-based segmentation, multi-domain feature extraction and class imbalance correction. A stacked ensemble model, comprising Random Forest and XGBoost, is employed to achieve robust multi-class classification across diverse vehicle types (Section 3.5). An overview of the proposed approach is illustrated in Figure 4.19.

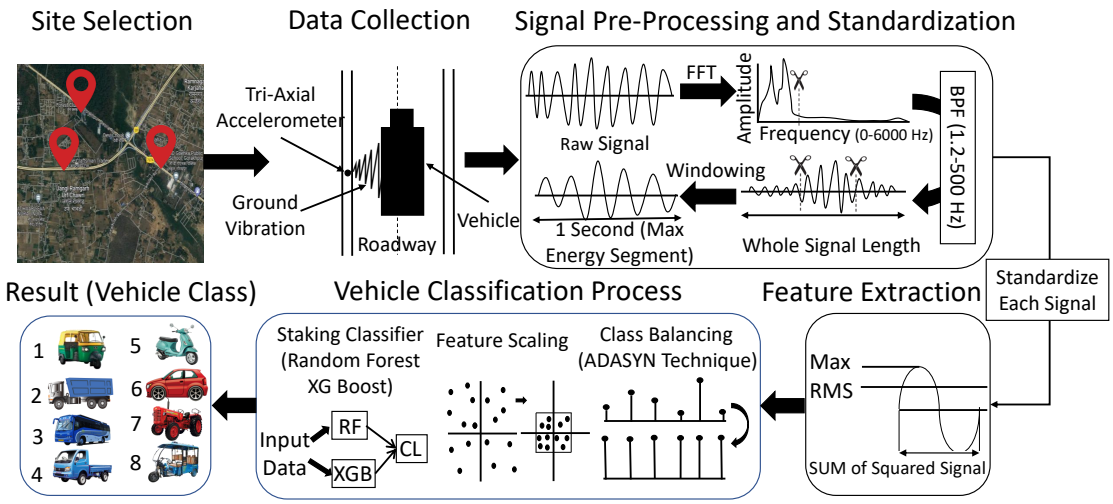

Fig. 4.19 An overview of the proposed approach.

Algorithm 1: RVEL and PCVE Modeling and Validation

Input: Vibration dataset of **9,257 single-vehicle pass-by events** including acceleration metrics, vehicle speed (S) and vehicle types (C);

Output: Trained RVEL models and computed PCVE values

1. Data Initialization and Loading

Load the dataset into a DataFrame using `pandas`;

2. Data Cleaning and Pre-processing

Apply Fast Fourier Transform (FFT) to each acceleration signal;

Apply a 2nd-order Butterworth Band-Pass Filter with passband $1.2\,\text{Hz} \leq f \leq 500\,\text{Hz}$;

Trim the first 700 ms of each filtered signal to remove distortion;

3. Data Binning and Averaging

Sort the dataset by vehicle speed S;

Segment speeds into bins of $\Delta S = 5\,\text{km/h}$ using a sliding window;

for *each bin* $B_i = [S_i, S_i + \Delta S)$ **do**

Calculate averaged metrics:

$$\overline{A}_{D,B_i} = \frac{1}{N_{B_i}} \sum_{j=1}^{N_{B_i}} A_{D,j}, \quad \overline{\text{RMS}}_{D,B_i} = \sqrt{\frac{1}{N_{B_i}} \sum_{j=1}^{N_{B_i}} (\text{RMS}_{D,j})^2}, \quad \overline{E}_{D,B_i} = \frac{1}{N_{B_i}} \sum_{j=1}^{N_{B_i}} E_{D,j}$$

Convert units: A_D and RMS_D from m/s^2 to mm/s^2, E_D to μW;

Remove bins with $N_{B_i} < 5$;

4. Model Building: RVEL

for *each vehicle class C and direction* $D \in \{X, Y, Z\}$ **do**

Define and train a linear regression model on the entire binned dataset:

$$V_{D,C} = \alpha_{D,C} \cdot S + \beta_{D,C} + \varepsilon_{D,C}$$

5. Model Validation

for *each trained RVEL model* **do**

Predict $V_{D,C}$ on the complete binned dataset;

Calculate evaluation metrics: R^2, MAE, RMSE, p-values and F-statistics;

Assess model performance based on high R^2 and low error metrics;

6. PCVE Calculation

for *each vehicle class* $C \neq C_{Car}$ *and direction* $D \in \{X, Y, Z\}$ **do**

Predict $V_{D,C}(S)$ using the corresponding RVEL model for various speeds S;

Compute PCVE as:

$$\text{PCVE}_{D,C}(S) = \frac{V_{D,C}(S)}{V_{D,C_{\text{Car}}}(S)}$$

7. Software Tool Development

Develop a Python-based application to predict PCVE and RVEL for user-input speed values;

Features:

- **User Input:** Select vehicle type, metric, direction and input speed S;
- **Computation:** Apply pre-trained RVEL models to compute $V_{D,C}(S)$ and $\text{PCVE}_{D,C}(S)$;
- **Visualization:** Display regression equations and prediction results through plots;
- **Integration:** Load regression parameters from external files;
- **Interface:** Provide an intuitive GUI for user interaction;

4.7.2 Motivation and Objectives

The present study introduces a novel vehicle classification framework utilizing a single tri-axial accelerometer. This configuration minimizes environmental sensitivity and deployment costs while maintaining high accuracy by applying a stacked ensemble classifier comprising Random Forest and XGBoost models. The primary objectives of this research are:

1. To develop a low-cost single-sensor classification system that is robust to environmental conditions,

2. To reduce installation complexity and associated costs

3. To enhance classification robustness and accuracy in class-imbalanced traffic scenarios

This approach offers a cost-effective and non-intrusive alternative capable of delivering consistent, high-accuracy vehicle classification, even in significant class imbalances, thus advancing state-of-the-art intelligent transportation systems.

4.7.3 Site Survey and Data Collection and Raw Signal Pre-Processing

The complete procedure encompassing site survey, instrumentation setup and signal preprocessing is uniform across all studies and has been described in detail under the RVEL and PCVE framework; refer to Section 4.6 for comprehensive methodological details.

A total of 9476 single-vehicle pass-by events were recorded as shown in Figure 4.20, spanning eight distinct vehicle classes: Truck (4391; 46.3%), 2-Wheeler (1908; 20.1%), Car/SUV (1763; 18.6%), Light Commercial Vehicle (LCV) (554; 5.8%), E-Rickshaw (301; 3.2%), Bus (289; 3.0%), Three-Wheeler (159; 1.7%) and Tractor (111; 1.2%). Each pass-by event captured acceleration measurements (m/s^2) from approach to departure,

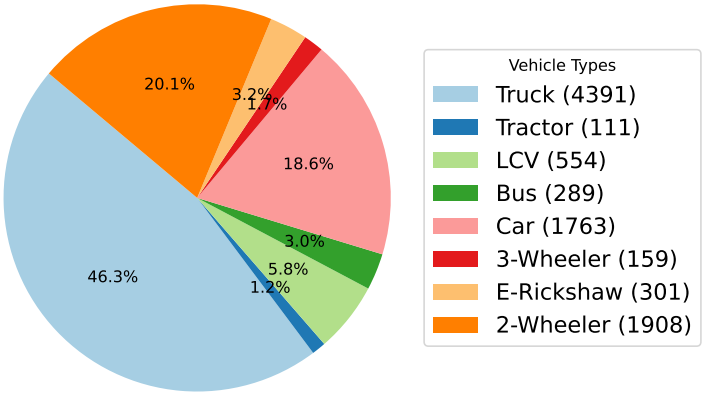

Fig. 4.20 Vehicle class-wise distribution in the dataset.

isolating its unique vibration signature. The data used in this study were extracted from the same experimental dataset directory; however, the number of usable events varies between studies due to differential outlier removal criteria applied to meet specific objectives.

4.7.4 Feature extraction from the maximum energy window

Various features are extracted from the window with the highest energy to characterize the signal. Key features are calculated from the maximum energy window $x_{k_{\max}}$:

- The peak value of the signal within the window: Max Amplitude $= \max_n |x_{k_{\max}}(n)|$. Maximum amplitude indicates the highest intensity of the signal in the window, which is essential for understanding the signal's peak behavior.
- A measure of the signal's power, given by: RMS $= \sqrt{\frac{1}{12800}\sum_{n=0}^{12799} x_{k_{\max}}(n)^2}$. RMS value provides an average measure of the signal's power and is less sensitive to outliers than maximum amplitude.
- The total energy within the window, reinforcing the energy calculation: $E_{\text{total}} = \sum_{n=0}^{12799} x_{k_{\max}}(n)^2$. The total energy directly indicates the signal's intensity over the window and helps in comparing different windows based on their energy content.

Extracting these features helps create a comprehensive signal profile within the window with the highest energy, which can be used for further analysis or classification. The table 4.8 represents the descriptive analysis of the whole data set; in this, Max and RMS values are in acceleration (m/s^2) and SUM (Signal Energy) values are in (m^2/s^4).

Table 4.8 Descriptive analysis of the data set class-wise.

Vehicle	Truck	Tractor	LCV	Bus	Car	3-W AUTO	E-Rickshaw	2-W
X Mean	0.033	0.055	0.025	0.048	0.024	0.024	0.027	0.023
X Std. Dev.	0.017	0.027	0.008	0.027	0.005	0.006	0.007	0.005
X Min	0.013	0.014	0.013	0.016	0.012	0.013	0.015	0.013
X Max	0.175	0.141	0.143	0.169	0.078	0.059	0.064	0.098
Y Mean	0.023	0.039	0.014	0.037	0.013	0.015	0.019	0.012
Y Std. Dev.	0.015	0.020	0.008	0.024	0.005	0.008	0.009	0.004
Y Min	0.008	0.011	0.009	0.009	0.008	0.009	0.009	0.008
Y Max	0.147	0.103	0.084	0.144	0.087	0.061	0.071	0.102
Z Mean	0.022	0.027	0.017	0.032	0.013	0.018	0.015	0.012
Z Std. Dev.	0.013	0.011	0.013	0.016	0.004	0.014	0.006	0.004
Z Min	0.009	0.012	0.008	0.009	0.008	0.009	0.009	0.008
Z Max	0.166	0.061	0.157	0.099	0.066	0.094	0.073	0.068
X RMS Mean	0.008	0.016	0.005	0.011	0.004	0.005	0.006	0.004
X RMS Std. Dev.	0.005	0.009	0.002	0.007	0.001	0.001	0.002	0.001
X RMS Min	0.003	0.004	0.003	0.003	0.003	0.003	0.003	0.003
X RMS Max	0.046	0.040	0.020	0.039	0.022	0.011	0.021	0.024
Y RMS Mean	0.006	0.012	0.004	0.009	0.003	0.004	0.005	0.003
Y RMS Std. Dev.	0.004	0.006	0.001	0.006	0.001	0.001	0.003	0.001
Y RMS Min	0.003	0.003	0.003	0.003	0.003	0.003	0.003	0.003
Y RMS Max	0.038	0.034	0.017	0.033	0.021	0.007	0.024	0.027
Z RMS Mean	0.006	0.007	0.004	0.007	0.003	0.004	0.004	0.003
Z RMS Std. Dev.	0.002	0.003	0.002	0.003	0.001	0.002	0.001	0.001
Z RMS Min	0.003	0.004	0.003	0.003	0.003	0.003	0.003	0.003
Z RMS Max	0.035	0.014	0.019	0.021	0.010	0.018	0.013	0.017
X SUM Mean	0.896	1.758	0.518	1.254	0.475	0.512	0.652	0.445

Continued on next page

Table 4.8 continued from previous page

Vehicle	Truck	Tractor	LCV	Bus	Car	3-W AUTO	E-Rickshaw	2-W
X SUM Std. Dev.	0.573	0.974	0.181	0.776	0.154	0.147	0.262	0.138
X SUM Min	0.195	0.224	0.195	0.199	0.197	0.208	0.209	0.193
X SUM Max	5.183	4.576	2.297	4.411	2.511	1.277	2.344	2.769
Y SUM Mean	0.704	1.309	0.417	0.995	0.384	0.401	0.616	0.367
Y SUM Std. Dev.	0.477	0.718	0.164	0.648	0.125	0.104	0.350	0.131
Y SUM Min	0.172	0.230	0.163	0.169	0.166	0.180	0.179	0.169
Y SUM Max	4.323	3.862	1.909	3.684	2.388	0.792	2.729	3.075
Z SUM Mean	0.639	0.787	0.457	0.799	0.354	0.468	0.453	0.361
Z SUM Std. Dev.	0.281	0.287	0.181	0.329	0.070	0.205	0.127	0.069
Z SUM Min	0.188	0.229	0.182	0.183	0.176	0.187	0.179	0.174
Z SUM Max	3.915	1.610	2.174	2.381	1.032	2.011	1.511	1.878

4.7.5 Class imbalance analysis and mitigation

Class imbalance is a significant challenge in machine learning, particularly in multi-class classification tasks. This imbalance can result in biased models favoring the majority classes, leading to poor performance in identifying and predicting the minority classes. To address this issue, this section examines the class distribution of the vehicle-type dataset before and after applying the ADASYN (Adaptive Synthetic Sampling) technique, which aims to create a more balanced dataset.

Initially, the class distribution of the dataset is highly imbalanced. For instance, the class 'Truck' has a significantly higher number of instances than the 'Tractor' class, as shown in Table 4.9. This imbalance is detrimental to the model's ability to learn and predict minority classes effectively. The ADASYN technique was employed to mitigate this, which generates synthetic instances for minority classes based on their feature space. This method ensures a more balanced representation of all classes in the dataset.

Table 4.9 Class distribution, counts and ratios before and after balancing using ADASYN.

Class	Count		Ratio	
	Before	**After**	**Before**	**After**
Truck	4391	4391	3.59	1.00
2-Wheeler	1908	4200	1.56	0.96
Car	1763	4499	1.44	1.03
LCV	554	4525	0.45	1.03
E-Rickshaw	301	4441	0.25	1.01
Bus	289	4297	0.24	0.98
3-Wheeler	159	4321	0.13	1.01
Tractor	111	4417	0.09	1.01

The Imbalance Ratio (IR) is a key metric quantifying a dataset's class imbalance degree. It is defined as the ratio of instances in the majority class to those in the minority class. The initial imbalance ratio in our dataset is calculated as follows:

$$IR = \frac{N_{majority}}{N_{minority}} = \frac{4391}{111} \approx 39.56. \tag{4.3}$$

This indicates a significant imbalance. After applying ADASYN, the dataset is much more balanced, as reflected in the new imbalance ratio: $IR = \frac{4525}{4200} \approx 1.08$. The average class size and the ratios for each class, both before and after balancing, were calculated for a comprehensive analysis.

Before Balancing

$$\text{Average class size} = \frac{(4391+1908+1763+554+301+289+159+111)}{8} = 1184.5.$$

After Balancing

$$\text{Average class size} = \frac{(4525+4499+4441+4417+4391+4321+4297+4200)}{8} = 4386.38.$$

The substantial increase in the average class size after balancing underscores the effectiveness of the ADASYN technique in generating synthetic samples to augment the minority classes (as shown in Table 4.9), achieving a more uniform distribution across all classes. Table 4.10 provides a structured overview of the experimental sets derived from different combinations of input variables and classification methods used in the vehicle classification study. The rows represent vibration-based features extracted from tri-axial acceleration signals, including root mean square (RMS), maximum value (Max) and summation of squared amplitudes (SUM) interpreted as signal energy. These are computed along various directional axes: X, Y, Z (individual axes), XY, XZ, YZ (pairwise combinations) and XYZ (all three axes combined).

The columns list six classifier configurations: WBS (With Data Balancing and Stacking), WBwSRF (With Data Balancing Without Stacking using Random Forest), WBwSXGB (With Data Balancing Without Stacking using XGBoost), wBWS (Without Data Balancing With Stacking), wBwSRF (Without Data Balancing Without Stacking using Random Forest) and wBwSXGB (Without Data Balancing Without Stacking using XGBoost). Each table cell corresponds to a uniquely indexed dataset (Set 1 to Set 126), combining a specific feature type with a classification strategy. For example, Set 1 uses XYZ RMS features with WBS, while Set 78 employs Y-axis Max with wBwSXGB. This systematic design supports comparative evaluation across all feature-method configurations.

This detailed examination of class distribution before and after balancing provides a clear depiction of the improvements brought by ADASYN. The balanced dataset is crucial for training machine learning models that are fair and accurate, especially in scenarios where the prediction of minority classes is as important as that of the majority classes.

Table 4.10 Distribution of sets with variables and methods.

Variables \ Methods	WBS	WBwSRF	WBwSXGB	wBWS	wBwSRF	wBwSXGB
XYZ RMS	Set 1	Set 2	Set 3	Set 4	Set 5	Set 6
XZ RMS	Set 7	Set 8	Set 9	Set 10	Set 11	Set 12
YZ RMS	Set 13	Set 14	Set 15	Set 16	Set 17	Set 18
XY RMS	Set 19	Set 20	Set 21	Set 22	Set 23	Set 24
X RMS	Set 25	Set 26	Set 27	Set 28	Set 29	Set 30
Y RMS	Set 31	Set 32	Set 33	Set 34	Set 35	Set 36
Z RMS	Set 37	Set 38	Set 39	Set 40	Set 41	Set 42
XYZ Max	Set 43	Set 44	Set 45	Set 46	Set 47	Set 48
XZ Max	Set 49	Set 50	Set 51	Set 52	Set 53	Set 54
YZ Max	Set 55	Set 56	Set 57	Set 58	Set 59	Set 60
XY Max	Set 61	Set 62	Set 63	Set 64	Set 65	Set 66
X Max	Set 67	Set 68	Set 69	Set 70	Set 71	Set 72
Y Max	Set 73	Set 74	Set 75	Set 76	Set 77	Set 78
Z Max	Set 79	Set 80	Set 81	Set 82	Set 83	Set 84
XYZ SUM	Set 85	Set 86	Set 87	Set 88	Set 89	Set 90
XZ SUM	Set 91	Set 92	Set 93	Set 94	Set 95	Set 96
YZ SUM	Set 97	Set 98	Set 99	Set 100	Set 101	Set 102
XY SUM	Set 103	Set 104	Set 105	Set 106	Set 107	Set 108
X SUM	Set 109	Set 110	Set 111	Set 112	Set 113	Set 114
Y SUM	Set 115	Set 116	Set 117	Set 118	Set 119	Set 120
Z SUM	Set 121	Set 122	Set 123	Set 124	Set 125	Set 126

4.7.6 Stacked classifier-based training

Stacked classifier-based training is a powerful ensemble method that can significantly enhance model performance by combining the outputs of multiple base classifiers. This approach can be efficient when the base models are diverse and capture different aspects of the data. Stacking involves training multiple base classifiers (*level-0 models*) and then using a meta-classifier (*level-1 model*) to combine their predictions. The goal is to leverage the strengths of different classifiers to achieve better overall performance. Stacked classifier-based training offers several key advantages. *Improved performance* is achieved by combining the strengths of different models, effectively mitigating the weaknesses of individual models. This ensemble approach leverages diverse classifiers to enhance predictive accuracy. *Robustness* is another significant benefit, as stacking multiple models reduces overfitting. By averaging out the errors of individual models, stacking lowers both

variance and bias, leading to more reliable predictions. Furthermore, stacking provides *flexibility* in model selection and combination. It allows for using a variety of base and meta-models, enabling customization and optimization for specific tasks and datasets. This flexibility makes stacked classifier-based training a powerful tool in machine learning.

After training the data with a stacking ensemble, the performance of the best classifier was evaluated and statistical significance was performed. In this regard, the complete training and testing process was repeated over multiple independent random splits to capture the variability inherent in the dataset. The accuracy obtained from each iteration was recorded and then analyzed to assess the consistency in performance. Statistical tests were employed to determine whether the observed performance improvements were robust and not merely due to chance.

Working Principal

The vehicle classification process initiates with the *input data*, represented as $\mathscr{D} = (\mathbf{X}, \mathbf{y})$, where $\mathbf{X} \in \mathbb{R}^{n \times d}$ denotes the feature matrix containing n samples and d features extracted from accelerometer signals and $\mathbf{y} \in \mathbb{R}^n$ is the corresponding target vector indicating vehicle classes. This data undergoes *data pre-processing*, which encompasses cleaning, normalization and encoding to ensure it is in an optimal format for model training. Formally, the pre-processing can be described by the transformation:

$$\mathscr{D}' = \text{Preprocess}(\mathscr{D}), \tag{4.4}$$

where $\mathscr{D}' = (\mathbf{X}', \mathbf{y}')$ represents the pre-processed dataset.

Subsequently, the pre-processed dataset is partitioned into training and validation subsets using a train-test split mechanism:

$$(\mathbf{X}_{\text{train}}, \mathbf{y}_{\text{train}}), (\mathbf{X}_{\text{valid}}, \mathbf{y}_{\text{valid}}) = \text{train\_test\_split}(\mathbf{X}', \mathbf{y}', \text{test\_size} = p), \tag{4.5}$$

where p denotes the proportion of data allocated to the validation set.

Base and Meta Classifiers

1. **Base Classifiers (Level-0 Models):** Multiple base classifiers are trained on the training dataset to capture diverse patterns within the data. This study employs a stacking framework comprising two base classifiers:

   - **Random Forest (h_1)**: Selected for their robustness and ability to handle large feature spaces through ensemble learning of decision trees.
   - **XGBoost Classifier (h_2)**: Chosen for its efficiency and superior performance in handling structured data with gradient boosting techniques.

2. **Generating Predictions**: Each base classifier h_i generates probabilistic predictions on both the training and validation sets:

$$\hat{\mathbf{y}}_{i,\text{train}} = h_i(\mathbf{X}_{\text{train}}), \quad \forall i \in \{1,2\}, \tag{4.6}$$

$$\hat{\mathbf{y}}_{i,\text{valid}} = h_i(\mathbf{X}_{\text{valid}}), \quad \forall i \in \{1,2\}. \tag{4.7}$$

   These predictions represent the probability estimates for each vehicle class, providing a foundation for the meta-classifier.

3. **Meta-Classifier (Level-1 Model)**: A meta-classifier H is trained on the meta-features derived from the base classifiers' predictions. In this study, Logistic Regression is utilized as the meta-classifier due to its simplicity and effectiveness in combining probabilistic outputs:

$$\hat{\mathbf{y}}_{\text{meta-train}} = H(\mathbf{Z}_{\text{train}}), \tag{4.8}$$

Where $\mathbf{Z}_{\text{train}} = [\hat{\mathbf{y}}_{1,\text{train}}, \hat{\mathbf{y}}_{2,\text{train}}]$ represents the concatenated predictions from the base classifiers on the training set.

Data Preparation

The collected vibration data, undergoes comprehensive pre-processing to ensure quality and suitability for model training. Pre-processing steps include:

- **Cleaning**: Removing noise and handling missing values to ensure data integrity.
- **Normalization**: Scaling features to a standard range to facilitate efficient model training and convergence. Mathematically, normalization can be expressed as:

$$\mathbf{X}' = \frac{\mathbf{X} - \mu}{\sigma}, \tag{4.9}$$

  where μ and σ represent the mean and standard deviation of the features, respectively.
- **Encoding**: Converting categorical variables into numerical formats if necessary, ensuring compatibility with machine learning algorithms. For instance, one-hot encoding transforms a categorical feature with k distinct values into k binary features.

After pre-processing, the dataset is split into training (80%) and validation (20%) subsets. The training set is used to build the base classifiers, while the validation set assesses their performance and facilitates the training of the meta-classifier.

Training Process

Each base classifier is trained on the training set to generate probabilistic predictions on both the training and validation sets:

$$h_i : \mathbf{X}_{\text{train}} \rightarrow \hat{\mathbf{y}}_{i,\text{train}}, \quad \forall i \in \{1,2\}, \tag{4.10}$$

where $\hat{\mathbf{y}}_{i,\text{train}}$ are the predicted probabilities for the training samples by the i-th base classifier.

The trained base classifiers generate predictions on the validation set:

$$\hat{\mathbf{y}}_{i,\text{valid}} = h_i(\mathbf{X}_{\text{valid}}), \quad \forall i \in \{1,2\}. \tag{4.11}$$

These predictions form the meta-features for the meta-classifier:

$$\mathbf{Z}_{\text{train}} = [\hat{\mathbf{y}}_{1,\text{train}}, \hat{\mathbf{y}}_{2,\text{train}}], \tag{4.12}$$

$$\mathbf{Z}_{\text{valid}} = [\hat{\mathbf{y}}_{1,\text{valid}}, \hat{\mathbf{y}}_{2,\text{valid}}]. \tag{4.13}$$

The meta-classifier H is then trained on the training meta-features:

$$H : \mathbf{Z}_{\text{train}} \rightarrow \hat{\mathbf{y}}_{\text{meta-train}}, \tag{4.14}$$

where $\hat{\mathbf{y}}_{\text{meta-train}}$ represents the predicted probabilities from the meta-classifier on the training meta-features.

Finally, the meta-classifier makes the final predictions on the validation set:

$$\hat{\mathbf{y}}_{\text{final}} = H(\mathbf{Z}_{\text{valid}}). \tag{4.15}$$

The performance of the stacked model is evaluated using metrics such as accuracy, precision, recall and F1 score:

$$\text{Accuracy} = \frac{\text{TP} + \text{TN}}{\text{TP} + \text{TN} + \text{FP} + \text{FN}}, \tag{4.16}$$

$$\text{Precision} = \frac{\text{TP}}{\text{TP} + \text{FP}}, \tag{4.17}$$

$$\text{Recall} = \frac{\text{TP}}{\text{TP} + \text{FN}}, \tag{4.18}$$

$$\text{F1 Score} = 2 \times \frac{\text{Precision} \times \text{Recall}}{\text{Precision} + \text{Recall}}, \tag{4.19}$$

where TP, TN, FP and FN denote true positives, true negatives, false positives and false negatives, respectively.

Adaptive Synthetic Sampling (ADASYN): Class imbalance is prevalent in vehicle classification datasets, where minority classes (e.g., e-rickshaws, specialized commercial vehicles) are underrepresented. ADASYN addresses this by generating synthetic samples for minority classes based on the density distribution of the feature space. The ADASYN algorithm can be formalized as:

$$\text{ADASYN}(\mathbf{X}, \mathbf{y}) = \mathbf{X}' \cup \{\mathbf{x}_s \mid \mathbf{x}_s \text{ is a synthetic sample generated for minority class}\}, \tag{4.20}$$

where $\mathbf{X}'$ is the augmented feature set after applying ADASYN.

Stacking Ensemble Mechanism: The stacking ensemble leverages the strengths of multiple classifiers to improve overall performance. The mathematical representation of the stacking mechanism is as follows:

$$\hat{\mathbf{y}}_{\text{final}} = H(\mathbf{Z}_{\text{valid}}) = H([h_1(\mathbf{X}_{\text{valid}}), h_2(\mathbf{X}_{\text{valid}})]), \tag{4.21}$$

where H learns to combine the base classifiers' predictions h_1 and h_2 to produce the final classification output.

Loss Function and Optimization: The classifiers are trained using loss functions that quantify the difference between predicted probabilities and actual labels. For instance, Logistic Regression employs the binary cross-entropy loss function:

$$\mathscr{L} = -\frac{1}{n}\sum_{i=1}^{n}\left[y_i \log(\hat{y}_i) + (1-y_i)\log(1-\hat{y}_i)\right], \tag{4.22}$$

where $\mathscr{L}$ is the loss function, y_i is the true label and $\hat{y}_i$ is the predicted probability. Regularization techniques are applied to prevent overfitting and enhance generalization. For example, L2 regularization can be incorporated into the loss function:

$$\mathscr{L}_{\text{reg}} = \mathscr{L} + \lambda \sum_{j=1}^{d} \theta_j^2, \tag{4.23}$$

where λ is the regularization parameter and θ_j are the model parameters.

Justification for Model Choices: Random Forest and XGBoost are selected as base classifiers due to their complementary strengths. Random Forest excels in handling high-dimensional data and capturing non-linear relationships through ensemble learning of decision trees. XGBoost, with its gradient boosting framework, offers efficient handling of structured data, regularization to prevent overfitting and robust performance in classification tasks. Combining these classifiers in a stacking ensemble leverages their advantages, enhancing overall classification accuracy and robustness.

4.7.7 Statistical Analysis of Model Performance

The performance of the vehicle classification model was evaluated using a series of statistical tests on the test accuracies obtained over multiple iterations. Let the array of test accuracies be represented by $\{x_1, x_2, \ldots, x_N\}$, where N denotes the number of iterations. The sample mean is computed as

$$\bar{x} = \frac{1}{N} \sum_{i=1}^{N} x_i,$$

and the sample standard deviation is calculated by

$$s = \sqrt{\frac{1}{N-1} \sum_{i=1}^{N} (x_i - \bar{x})^2}.$$

To quantify the uncertainty in the estimated mean accuracy, a 95% confidence interval is constructed using the Student's t-distribution:

$$\bar{x} \pm t_{\alpha/2, N-1} \cdot \frac{s}{\sqrt{N}},$$

where $t_{\alpha/2, N-1}$ is the critical value from the t-distribution with $N-1$ degrees of freedom at a significance level $\alpha = 0.05$.

Furthermore, a one-sample t-test is performed to evaluate whether the mean test accuracy differs significantly from a predetermined benchmark value μ_0. The t-statistic for this test is computed as

$$t = \frac{\bar{x} - \mu_0}{s/\sqrt{N}},$$

and the resulting p-value is used to assess the statistical significance of any deviation.

Finally, the density distribution of the test accuracies is visualized using kernel density estimation (KDE), with the mean and the boundaries of the 95% confidence interval

superimposed on the plot. This comprehensive statistical framework ensures that the model's performance is validated and its consistency and reliability are well established.

4.7.8 System Parameters

The system parameters used in this study are summarized in Table 4.11. The experimental setup includes a tri-axial accelerometer with a sampling frequency of 12.8 kHz per axis. A 2nd-order Butterworth band-pass filter (1.2-500 Hz) was applied to preprocess the signals, ensuring accurate vibration analysis.

Table 4.11 System Parameters Used in the Study

Category	Parameter	Specification / Description
Hardware	Sensor	Single tri-axial accelerometer (01dB ACOEM)
	Sampling Frequency	12.8 kHz per axis
	Frequency Range	6 kHz (factory-calibrated, up to 80 g)
	Full-Scale Range	Up to 80 g
	Mounting	Custom mounting device (patent pending), flush on pavement
Data Collection	Recording Format	`.CMG` files
	Duration	Approx. 20 days of single-vehicle pass-by events
	Traffic Condition	Manually triggered to isolate single-vehicle vibrations
	Environment	Dry, bituminous pavement, no major potholes
Signal Processing	Filter	2nd-order Butterworth band-pass, 1.2–500 Hz
	Windowing	Rectangular window (700 ms) to remove filter transients
	Segmentation	1-second window capturing maximum signal energy
	Axes Analyzed	X, Y and Z directions
Feature Extraction	RMS Value	Root Mean Square acceleration in each axis
	Peak Value	Maximum acceleration amplitude in each axis
	Total Energy	summation of squared accelerations per axis
	Axis Combinations	Single axes (X, Y, Z), or pairs/triplets (XY, YZ, XZ, XYZ)
	Polynomial Features	Quadratic interaction terms (`degree=2`, `interaction_only=True`)
Machine Learning	Class Balancing	ADASYN (`random_state=42`) to oversample minority classes
	Classifiers	Random Forest + XGBoost in the stacked ensemble
	Meta-Classifier	Logistic Regression (`max_iter=10000`, `solver=liblinear`)
	Data Split	60% training, 20% validation, 20% test
	Cross-Validation	5-fold (`cv=5`), scoring=`'accuracy'`
	Experiment Repetitions	50 independent iterations with repeated random splits
	Statistical Analysis	One-sample t-test
	Libraries	Python 3.X, `scikit-learn`, `xgboost`, `imblearn`
Runtime / Environment	Distribution	Anaconda 2.4.2 (with Jupyter Notebook)
	Operating System	Windows 11 (64-bit)
	Hardware	Typical CPU e.g., Intel i7, 16 GB RAM
	Runtime	200–230 seconds for the best-performing set

4.7.9 Vibration Signals to Vehicle Classification Algorithm

The vibration-to-vehicle classification algorithm (Algorithm 2) is developed to classify vehicles solely based on the vibrations they generate while traversing the roadway. This approach leverages the intrinsic vibrational fingerprint of each vehicle type, offering a non-intrusive, sensor-based classification alternative. The process begins by loading a vibration signal dataset into a *Data Frame*, where independent variables (features) and the target variable (vehicle type) are explicitly defined.

To improve model performance, the algorithm applies *polynomial features* to enrich the feature space and uses feature scaling to standardize input distributions, reducing sensitivity to magnitude differences. Depending on the experimental condition, the dataset is either balanced using the ADASYN algorithm to address class imbalance or used directly in its original distribution. Importantly, the balancing step ensures that underrepresented vehicle categories are sufficiently represented during model training, improving generalization.

The data is then split into training, testing and validation sets, providing a structured pipeline for robust model evaluation. Four distinct training configurations are implemented: with or without ADASYN balancing and with or without stacking classifiers. In the stacking setup, ensemble methods combining Random Forest and XGBoost classifiers are employed to capture both non-linear and gradient-boosted decision boundaries. Alternatively, single classifier models are trained under the unbalanced approach for comparison.

Model performance is assessed using metrics such as the confusion matrix, accuracy, AUC-ROC, precision and recall, ensuring comprehensive classification evaluation. The modular design allows integration of alternative features, ensemble models, or balancing methods, making it adaptable to diverse datasets and evolving needs. This flexibility enhances the framework's scientific robustness and broadens its application scope.

Algorithm 2: Vibration to vehicle classification algorithm.

Input: Vibration dataset of the single-vehicle pass-by;

Initialization and Data Loading

Load dataset into a DataFrame using: df = pd.read_excel($\cdot$);

Define independent variables X and target variable y:
$X = \text{df}[\text{independent\_vars}], y = \text{df}[\text{'vehicle\_type'}]$;

Data Processing and Feature Engineering

Apply Polynomial Features: $X_{\text{poly}} = \text{PolynomialFeatures}(\cdots).\text{fit\_transform}(X)$;

Scale the features: $X_{\text{scaled}} = \text{StandardScaler}().\text{fit\_transform}(X_{\text{poly}})$;

Data Balancing

If the method includes balancing (***function*** *bal1()* and **function** bal2()), apply ADASYN:
$(X_{\text{resampled}}, y_{\text{resampled}}) = \text{ADASYN}(\text{random\_state} = 42).\text{fit\_resample}(X_{\text{scaled}}, y)$;

If the method does not include balancing (***function*** *bal3() and* ***function*** *bal4()*), use the scaled data directly: $X_{\text{resampled}} = X_{\text{scaled}}, y_{\text{resampled}} = y$;

Data Splitting

Split the data into training and test sets:
$(X_{\text{train}}, X_{\text{test}}, y_{\text{train}}, y_{\text{test}}) = \text{train\_test\_split}(X_{\text{resampled}}, y_{\text{resampled}}, \cdot, \cdot)$;

Further, split the training data into training and validation sets:
$(X_{\text{train}}, X_{\text{val}}, y_{\text{train}}, y_{\text{val}}) = \text{train\_test\_split}(X_{\text{train}}, y_{\text{train}}, \cdot, \cdot)$;

Model Evaluation

Predict the target variable for the test set using the trained models:
$y_{\text{pred}} = \text{model.predict}(X_{\text{test}})$;

Calculate evaluation metrics:

Confusion Matrix: conf_matrix = confusion_matrix$(y_{\text{test}}, y_{\text{pred}})$;

Accuracy: accuracy = accuracy_score$(y_{\text{test}}, y_{\text{pred}})$;

AUC-ROC:
auc_roc = roc_auc_score$(y_{\text{test}}, \text{model.predict_proba}(X_{\text{test}}), \text{multi_class} = \textit{'ovr'})$;

Precision: precision = precision_score$(y_{\text{test}}, y_{\text{pred}}, \text{average} = \textit{'weighted'})$;

Recall: recall = recall_score$(y_{\text{test}}, y_{\text{pred}}, \text{average} = \textit{'weighted'})$;

return Trained model for vehicle classification;

Model Definition and Training

function *bal1()* /*With Balancing With Stacking */
  base_learners = [('rf', RandomForestClassifier($\cdot$), ('xgb', XGBClassifier($\cdot$)];
  stacking_clf = StackingClassifier(estimators = base_learners, final_estimator = LogisticRegression(max_iter));
  stacking_clf.fit$(X_{\text{resampled}}, y_{\text{resampled}})$;

function *bal2()* /*With Balancing Without Stacking*/
  Train RandomForestClassifier: rf_clf.fit$(X_{\text{resampled}}, y_{\text{resampled}})$;
  Train XGBClassifier: xgb_clf.fit$(X_{\text{resampled}}, y_{\text{resampled}})$;

function *bal3()* /*Without Balancing With Stacking*/
  base_learners = $[('rf', \text{RandomForestClassifier}(\cdot)), ('xgb', \text{XGBClassifier}(\cdot))]$;
  stacking_clf = StackingClassifier(estimators = base_learners, final_estimator = LogisticRegression(max_iter));
  stacking_clf.fit$(X_{\text{train}}, y_{\text{train}})$;

function *bal4()* /*Without Balancing Without Stacking*/
  Train RandomForestClassifier: rf_clf.fit$(X_{\text{train}}, y_{\text{train}})$;
  Train XGBClassifier: xgb_clf.fit$(X_{\text{train}}, y_{\text{train}})$;

4.8 Route Optimization and Traffic Forecasting Using an Augmented Machine Learning Framework

4.8.1 Introduction

This study introduces a two-stage machine learning-based overlay framework (Section 3.6) designed to enhance road traffic prediction and optimize vehicular routing in mixed urban traffic environments. The schematic overview of the proposed methodology is illustrated in Figure 4.21, which highlights both the training and testing stages of the framework.

In the training stage, classified vehicle volume data is collected from selected urban road segments and preprocessed through a series of operations, including detrending for stationarity, anomaly detection and removal, regularization of sampling frequency and missing data imputation. Two forecasting models, Auto-Regressive Integrated Moving Average (ARIMA) and Support Vector Machine (SVM), are trained to learn traffic volume patterns over time.

In the testing stage, the outputs from these forecasting models are augmented with GPS data corresponding to the same spatio-temporal intervals. The combined dataset is annotated with traffic condition labels (Excellent, Good and Worse) and used to train an Extreme Gradient Boosting (XGBoost) classifier. The trained model enables real-time traffic condition prediction based on incoming GPS coordinates and forecasted traffic states.

The complete methodology spanning from data acquisition and preprocessing to model training and classification is detailed in Algorithm 3 and serves as the foundation for developing intelligent traffic-aware navigation systems.

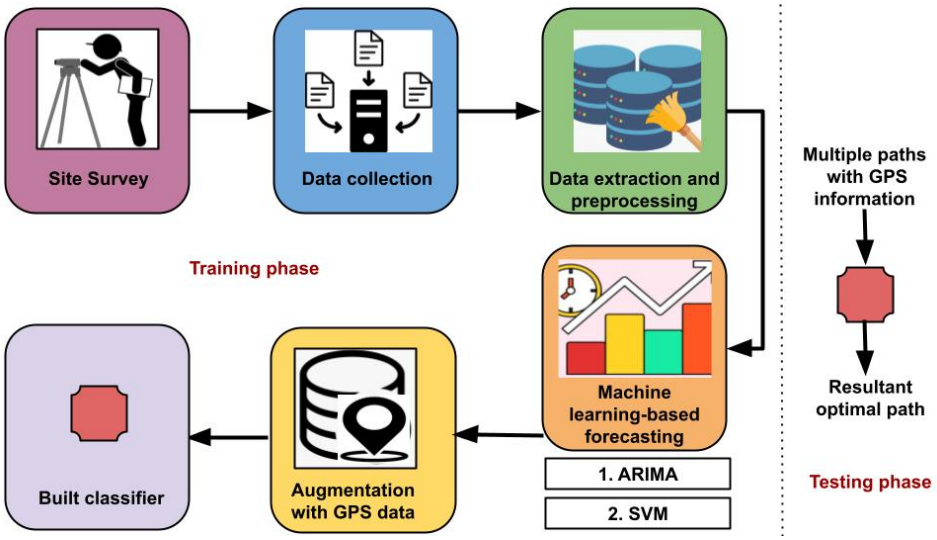

Fig. 4.21 Overview of the proposed machine learning-based overlay framework for traffic forecasting and route optimization. The training and testing phases are shown.

4.8.2 Motivation and Objectives

Accurate traffic forecasting in heterogeneous traffic environments remains challenging due to the variability of vehicle classes and sparse real-time data. Existing GPS-based systems often neglect classified vehicle volume, leading to limited prediction accuracy. Bridging this gap through integrated forecasting and spatial augmentation is essential for data-driven traffic management.

The primary objectives of this study are:

- To develop a hybrid forecasting framework combining ARIMA and SVM models on classified vehicle volume data.
- To augment time-series forecasts with GPS data for location-specific traffic condition prediction.
- To train an XGBoost classifier for real-time classification of traffic states using the augmented dataset.

Fig. 4.22 A snapshot of the recording site at Varanasi.

4.8.3 Site Survey and Data Collection

The complete site survey methodology, including location selection criteria, peak hour identification and field validation, has already been described in Section 4.3.2. The current study utilizes the same survey framework to ensure consistency in site geometry and traffic observation conditions across both cities.

4.8.4 Data collection

After site selection, video recording data was collected using high-quality cameras. At each site, six rounds of data were collected and each round consisted of three peak hours based on traffic (*i.e.,* morning peak, evening peak and off-peak). The mid-block locations of two-lane roads were identified to estimate the traffic volume. The sixth round specifies that the readings were taken six times in the morning, evening and off-peak. The site was identified by the local people's survey and analysis of Google map data. In addition, the traffic departments of Varanasi and Gorakhpur were consulted to identify traffic-prone zones during morning and evening peak hours. A snapshot of one of the data recording sites is shown in Fig. 4.22.

4.8.5 Data extraction and pre-processing

In data extraction and annotation, the classified vehicle volume was manually counted from the videos recorded during data collection. The video counting was carried out for each 15 minute out of one hour of peaks. Vehicles are divided into 12 distinct categories, *i.e.,* 2-w (two-wheelers), 3-w (three-wheelers), Car, Jeep/SUV, LCV (light commercial vehicle), Tractor, Bus, Truck, Rickshaw, E-Rickshaw, bicycle and others. To perform appropriate annotation, volunteers were appointed to manually count the vehicles and their categories from the recorded video; counting was done separately for both roadway directions. It is tedious to perform data processing for time series forecasting. The forecasting using simple rolling averages to long-shot term memory models requires immaculate data time series. Therefore, this work uses the following data-cleaning steps before forecasting and augmentations. The discussed steps are generally effective in working on our collected dataset. This work also provides the room to apply other data-cleaning techniques depending on the level of noise or uncertainty in the dataset.

- **Detrending/ Stationarity:** The proposed technique generates the mean-variance stationary time series from the raw input series in the first data-cleaning stage. This implies that the statistical properties of the built forecasting model remain invariant in the number of samples taken for the training. Generally, the forecasting model built using stationary data holds robustness properties. It is obtained by using differencing.

- **Anomaly detection:** The outliers were identified and normalized in the data-cleaning stage before training a forecasting model. This is because the presence of an outlier in the data might zag the results from the forecasting models.

- **Identifying the sampling frequency:** Checking the sampling frequency of the raw data is a crucial step in determining the regularity of sampling. This work removes

the data generated due to irregular sampling or makes it uniform before applying any modeling techniques. It is mandatory because the irregular sampling breaks the time series into disjoint parts and may not superimpose with the forecasting model.

- **Missing data detection:** Finally, the proposed technique handles the missing data from the time series data. The moving average method was used to rectify the missing values from the series.

4.8.6 Machine learning-based forecasting of traffic volume

This section discusses the essential part of the proposed technique. It discusses the forecasting models, *i.e.,* ARIMA and SVM. Here, ARIMA and SVM models are strategic choices intended to leverage the strengths in the classification and prediction of the overlay technique. Next, the ARIMA model is well-suited for capturing time-series patterns and trends, which are critical for the present analysis involving collected time-series data. Further, the SVM model excels in handling nonlinear relationships and complex patterns within the data. Using ARIMA and SVM enhances the robustness and accuracy of predictions, as each model contributes distinct insights and addresses different dataset characteristics. Furthermore, various models were considered during the experimental phase; however, adequate performance was observed only with ARIMA and SVM. These models (ARIMA and SVM) allow us to achieve a more comprehensive understanding of the underlying dynamics and patterns that persist in the data, ultimately improving the reliability and generalizability of our study's findings. Further, this section provided background for data augmentation with GPS and helped construct the XGBoost classifier.

ARIMA model

This work employs the most widely used linear time series forecasting model, *i.e.,* Auto-Regressive Integrated Moving Average (ARIMA) [258]. The model is assumed to achieve

higher importance in real-world scenarios; thus, ARIMA was used to forecast the traffic volume using the previously collected dataset. ARIMA compresses three main parts: Auto-Regressive (AR), Integrated (I) and Moving Average (MA) [258].

1. **Auto-Regressive:** The sub-part Auto-Regression (AR) forecasts the variable of interest, *i.e.,* traffic volume on a particular site, using a linear combination of the previous value of variables. Specifically, the AR part implies that it is a regression of the variable against itself, *i.e.,* lagged values of the target variable as our input variables to forecast values for the future.

2. **Integrated:** The sub-part Integrated (I) in ARIMA defines the differencing, which must be applied to make the data instances stationary. In other words, the data values are replaced with the difference between the current and previous values.

3. **Moving Average (MA):** The sub-part Moving Average (MA) employs the dependency between an observation and a residual error from a moving average model applied to lag observations.

ARIMA Parameters: The sub-parts in the ARIMA are parameterized using the standard notations. Let $\mathscr{P}$, $\mathscr{Q}$ and $\mathscr{R}$ denote the standard notations of the ARIMA, where integer values substitute for the parameters to indicate the type of ARIMA.

- $\mathscr{P}$ denotes the lag observations in the ARIMA order, *i.e.,* lag order.
- $\mathscr{Q}$ represents the differenced count of raw operations, *i.e.,* degree of difference.
- $\mathscr{R}$ denotes the window size of moving average, *i.e.,* order of moving average.

For example, a zero value is used as a parameter, which implies particular sub-parts are not used in the ARIMA model. Therefore, the ARIMA model is easily constructed to perform the function of an ARIMA model or even, specifically, AR, I, or MA models.

Mathematical structure of ARIMA

The mathematical structure of the ARIMA model used in this work, is inspired from [259] and discussed as follows. The ARIMA model relies upon the two terms, AR and MA, discussed earlier. It is assumed that the AR term represents the first difference and the MA term moderates the first difference. Thus, a redundant pair of these two terms will cancel out each other. More precisely, the first MA order is equivalent to a high AR order. To prove this underlying dependency, this work discusses the mathematical structure of ARIMA specific to traffic volume prediction. Let $\mathbf{B^s}$ represent the back-shift operator in the ARIMA. It performs the backwards shifting operation of multiplication by one period in time. In other words, for a given time series, denoted as $\mathbb{T}_t^s$, at time t, the following expression was obtained:

$$\mathbf{B^s}\mathscr{T}_t^s = \mathscr{T}_{t-1}^s. \tag{4.24}$$

The higher powers multiplication on $\mathbf{B^s}$ corresponds to yields a backward shift of more than one period shift in traffic volume prediction, as:

$$(\mathbf{B^s})^2\mathscr{T}_t^s = \mathbf{B^s}(B\mathscr{T}_t^s) = \mathbf{B^s}(\mathscr{T}_{t-1}^s) = \mathscr{T}_t^s - 2. \tag{4.25}$$

Similarly, for n intermediate values, the following expression was obtained:

$$(\mathbf{B^s})^n\mathscr{T}_t^s = \mathscr{T}_{t-n}^s. \tag{4.26}$$

From above, multiplication by $\mathbf{B^s}$ with the n^{th} power shits the observation backwards by n periods. The first difference operation can be simply represented using the term $\mathbf{B^s}$.

Let $\mathbb{T}^s$ denote the first difference of $\mathscr{T}^s$. Thus, for any t, the expression is as follows:

$$\mathbb{T}_t^s = \mathscr{T}_t^s - \mathscr{T}_t^s - 1 = \mathscr{T}_t^s - \mathbf{B^s}\mathscr{T}_t^s = \left(1 - \mathbf{B^s}\right)\mathscr{T}_t^s. \tag{4.27}$$

The above equation implies the difference series $\mathbb{T}_t^s$ can be easily derived from the series $\mathscr{T}_t^s$ using the factor of $1 - \mathbf{B^s}$. Let Z^s is the first difference of $\mathbb{T}^s$, *i.e.,* Z^s is the second difference of $\mathscr{T}^s$. The expression can be written as:

$$Z_t^s = \mathbb{T}_t^s - \mathbb{T}_{t-1}^s = \left(1 - \mathbf{B^s}\right)\mathbb{T}_t^s = \left(1 - \mathbf{B^s}\right)\left(\left(1 - \mathbf{B^s}\right)\mathscr{T}_t^s\right) = \left(1 - \mathbf{B^s}\right)^2\mathscr{T}_t^s. \tag{4.28}$$

The above equation indicates that the second difference of $\mathscr{T}^s$ can be obtained via multiplication of the $(1 - \mathbf{B})^2$ factor. Similarly, for p-order difference of $\mathscr{T}^s$ can be obtained by multiplying $(1 - \mathbf{B^s})^p$. Here, manipulating the shifting operation is a numeric variable in the above equation. It is true that the operator $\mathbf{B^s}$ is linear. Further, considering the ARIMA$(1,1,1)$ model for the time series $\mathscr{T}^s$ armed with the operator $\mathbf{B^s}$. The constant terms are omitted from the above-discussed ARIMA model to provide ease of representation and convenient readability. Thus, ARIMA$(1,1,1)$ can be defined by using the following pair of equations:

$$\mathscr{T}_t^s = \mathbb{T}_t^s - \mathbb{T}_{t-1}^s. \tag{4.29}$$

$$\mathscr{T}_t^s = \Omega_1\mathscr{T}_{t-1}^s + \mathscr{E}_t - \delta_1\mathscr{E}_{t-1}. \tag{4.30}$$

where $\mathscr{E}_t$ denotes the random noise at time t.

Now, using the back shift operation in ARIMA, the equation is updated as:

$$\mathscr{T}_t^s = (1 - \mathbf{B^s})\mathbb{T}_t^s \tag{4.31}$$

$$\mathbb{T}_t^s = \Omega_1 \mathbf{B^s} \mathscr{T}_t^s + \mathscr{E}_t - \delta_1 \mathbf{B^s} \mathscr{E}_t. \tag{4.32}$$

Now aggregation $\mathscr{T}^s$ on left and $\mathscr{E}$ on the right, the Eq. 4.32 can be repressed as:

$$(1 - \Omega \mathbf{B^s})\mathbb{T}_t^s = (1 - \delta_1 \mathbf{B^s})\mathscr{E}_t. \tag{4.33}$$

Now substitute the value of $\mathbb{T}_t^s$ in the definition of $\mathscr{T}_t^s$ to obtain a single equation, which involves $\mathscr{T}_t^s$ and $\mathscr{E}_t$. It summaries the ARIMA$(1,1,1)$ model and represented as:

$$(1 - \Omega_1 \mathbf{B}^s)(1 - \mathbf{B^s} \mathscr{T}_t^s = (1 - \delta_1 \mathbf{B^s})\mathscr{E}_t. \tag{4.34}$$

Here is the basic or mean ARIMA model, where the mean is assumed to be zero for traffic volume prediction. Thus, the model asserts that it is stationary white Gaussian noise, *i.e.,*: $\mathscr{T}_t^s = \mathscr{E}_t$. The above-discussed model is an ARIMA $(0,0,0)$ model; thereafter, ARIMA $(1,1,1)$ is obtained using a similar procedure. ARIMA $(1,1,1)$ uses different $\mathscr{T}_t^s$ and $\mathscr{E}_t$ to derive the expression. Specifically, the following properties are to be included: a) it involves a first difference by multiplying $\mathscr{T}_t^s$ with $(1 - \mathbf{B^s})$, b) it includes AR (1), which is equivalent to multiplying $\mathscr{T}_t^s$ by $(1 - \Omega_1 \mathbf{B^s})$ and c) it involves an MA (1) term, which is similar as multiplication of $\mathscr{E}_t$ by $(1 - \delta_1 \mathbf{B^s})$. From the above analysis of the ARIMA model, the following conclusion can be drawn:

- For AR (1) coefficient Ω_1 the factor $(1 - \Omega_1 \mathbf{B^s})$ on the left side is nearly equal to the factor $(1 - \mathbf{B^s})$. Further, each factor $(1 - \mathbf{B^s})$ appearing on the left side denotes the order of differencing. Therefore, AR (1) simply mimics an additional difference when the estimated coefficient$\rightarrow 1$.

- For MA (1) coefficient, denoted as $\delta_1 \to 1$, the factor $(1-\delta_1 \mathbf{B}^s)$ on the right side of the ARIMA equation is fairly the same as $(1-\mathbf{B}^s)$. If the factor $(1-\mathbf{B}^s)$ on the left side is cancelled by $(1-\delta_1 \mathbf{B}^s)$ on the right. It indicates MA (1) seamlessly reduces the difference order if the estimated coefficient $\to 1$.

- Let us consider the estimated AR(1) coefficient Ω_1 is equal to the estimated MA (1) coefficient δ_1. The factor of $\left(1-\Omega_1 \mathbf{B}^s\right)$ on the left of the ARIMA equation cancels $\left(1-\delta_1 \mathbf{B}^s\right)$ on the right. It implies that neither AR (1) and MR (1) terms belong to the model in the first place. Moreover, it also indicates that both terms are redundant.

SVM model

This sub-section discusses the Support Vector Machine (SVM)-based forecasting model used to predict the density of the traffic in an area at a particular time. SVM tries to obtain an optimal hyperplane separation between the classes in the traffic volume prediction training dataset. SVM is widely applicable and a powerful tool for classification and regression problems, as it avoids the over-fitting problem. In the case of binary classification, the SVM partitioned the data into classes 0 and 1. Similarly, for multi-class classification problems, the boundaries are drawn among multiple classes. Moreover, there are two SVM extension techniques for multi-class classification, *i.e.,* One Against All (OAA) and One Against One (OAO). Such techniques are most frequent and widely used for multi-class classification problems, as in the proposed work of traffic volume prediction. They rely on the factors of deducing the multi-class problem into a binary one. In other words, the multi-class classification problem is broken into multiple binary classification problems. Furthermore, the main idea of the SVM is to map the data $\mathscr{D}$ to a high-dimensional feature space via a nonlinear mapping; thereafter, performing a linear regression in the feature space.

Let us assume a training set having n data points, denoted as $\left\{\mathbf{x}_i, y_i\right\}_{i=1}^{n}$, where $\mathbf{x}_i \in |\mathscr{D}|$, $|\mathscr{D}|$ is the total number of data instances for traffic volume and output $y_i \in \mathbf{Y}$. The main motive behind applying the SVM model for load forecasting is to identify an optimal classification boundary, which makes a minimum loss on all the data instances. The regression function of SVM is as follows:

$$\mathscr{F}(x) = \omega\psi(x) + d_f, \tag{4.35}$$

where ω, d_f and $\psi(x)$ are the weights, offset and nonlinear mapping functions, respectively.

The transformation of the SVM for traffic volume prediction involves the solution of the following optimization problem, where the loss function construction involves a combination of the idea of structural risk minimization:

$$\min \quad \frac{1}{2}\|\omega\|^2 + \Pi_1 \sum_{i=1}^{n} \left(p_i + p_i^*\right), \tag{4.36a}$$

$$\text{s.t.,} \quad y_p - \omega\psi(x_i) - b \leq q_o + p_i, \tag{4.36b}$$

$$y_p + \omega\psi(x_i) + b \leq q_o + p_i^*, \tag{4.36c}$$

$$p_i \geq 0, p_i^* \geq 0, \tag{4.36d}$$

where, Π_1, p_i, p_i^* are penalty parameter and relative variables, respectively. The kernel function is defined as follows:

$$\mathscr{K}(x_i, x_j) = \psi(x_i)\psi(x_j). \tag{4.37}$$

Let g denote the variance in the kernel function and the RBF kernel is discussed as follows:

$$\mathscr{K}(x_i, x_j) = e^{(-g\|x_i - x_j\|^2)}. \tag{4.38}$$

4.8.7 Augmentation with GPS Data

This sub-section discusses the GPS segmentation technique, where predicted traffic volume is merged with GPS coordinates to enhance the performance of GPS-based navigation systems. Moreover, GPS-based augmentation acts as a mechanism to improve existing systems by enhancing performance, accuracy, availability, or other critical parameters, ultimately raising the precision of positioning, navigation and timely execution. In other words, such augmentation is not inherently part of the core GPS system but functions as an external overlay, complementing the existing framework to increase its overall effectiveness and reliability. GPS-based augmentation is widely adopted and has demonstrated impressive performance across public and private sectors, including transportation, logistics and emergency services. Various agencies and industries have embraced these augmentations to fulfill specific operational or regulatory requirements, achieving notable improvements in service quality and user experience.

For example, an augmented system can significantly improve the precision of the GPS satellite navigation system by reducing errors on the GPS clock and mitigating delays caused by adverse atmospheric conditions, multipath effects, or satellite geometry limitations. In this study, the augmentation with GPS data can be formally understood as:

$$\mathscr{D}_t = \mathscr{D}_f + \mathscr{D}_{GPS}, \tag{4.39}$$

Where $\mathscr{D}_t$, $\mathscr{D}_f$ and $\mathscr{D}_{GPS}$ represent the training dataset after augmentation, the forecasted dataset obtained from the SVM/ARIMA models and the raw GPS data, respectively. This augmented dataset $\mathscr{D}_t$ is further annotated and used to train an XGBoost model, as detailed in the next section. The trained model constructs a classifier capable of accurately predicting the traffic condition associated with each augmented data instance, enhancing the robustness and precision of the traffic forecasting system.

Algorithm 3: Improving the Mechanism of Road Traffic Prediction.

Input: GPS coordinates of $\mathscr{N}$ pre-specified locations;
Initialization: $n \leftarrow 1$;
Identify $\mathscr{N}$ sites for collecting dataset;
    This work considered $\mathscr{N} = 24$ sites; /*Section 4.3.2*/
while $(n \leq \mathscr{N})$ **do**
    $d \leftarrow$ Collect traffic volume data from site n;
    Dataset $\mathscr{D} \leftarrow append(d)$;
Final collected data is stored in $\mathscr{D}$;
Perform following operations on $\mathscr{D}$;
  (a) *Detrending/Stationarity*;
  (b) *Anomaly detection*;
  (c) *Identify the sampling frequency*;
  (d) *Missing data detection*;
Final preprocessed dataset $\mathscr{D}$;
Choose the forecasting model ($''0'' \rightarrow$ ARIMA and $''1'' \rightarrow$ SVM);
if *model* $==$ 0 **then**
    Estimate $\mathscr{P}$, $\mathscr{Q}$ and $\mathscr{R}$; /* as discussed in Section 4.8.6*/
    Train the ARIMA model for forecasting on $\mathscr{D}$;
else if *model* $==$ 1 **then**
    Train SVM-based forecasting model on on $\mathscr{D}$;
else
    No appropriate model is selected;
Obtain training dataset from $\mathscr{D}$ as $\mathscr{D}_f$;
Obtain GPS data in correspondence with $\mathscr{D}_f$, denoted as $\mathscr{D}_{GPS}$;
Augment $\mathscr{D}_f$ and $\mathscr{D}_{GPS}$ to obtain training data $\mathscr{D}_t$;
Annotate each instance of $\mathscr{D}_t$ under three types of labels;
Good (c_g), Worse (c_w) and Excellent (c_e);
Train XGBoost model on the annotated dataset to build the classifier;
A classifier can predict the appropriate traffic situation of a pre-specified area using:
 GPS data and **forecasted data** from **ARIMA** or **SVM** model ;
return XGBoost-based classifier to predict traffic conditions using GPS data and time;

4.8.8 Model training and building classifier

This sub-section discusses the construction of a classifier by training the XGBoost model using the augmented training dataset ($\mathscr{D}_t$) obtained in the previous section. In doing so, the proposed approach first annotates data instances of $\mathscr{D}_t$ as good, worse and excellent, denoted as c_g, c_w and c_e, respectively. To annotate an instance i in $\mathscr{D}_t$, a human-based approach was involved, where multiple volunteers manually assign c_g, c_w, or c_e labels. Moreover, the proposed approach also provides the opportunity to add automation in the annotation, which will be covered in the future. The annotated training dataset $\mathscr{D}_t$ is

supplied as input to the XGBoost [260] model to train a classifier π. The trained classifier (π) can easily detect the traffic volume using GPS data and forecasted value from the ARIMA or SVM model of a particular site among $\mathscr{N}$ identified sites.

This work uses XGBoost to perform domain-dependent data analysis and feature engineering. As it plays an important role in this work; therefore, XGBoost is our consensus choice to elaborate on the impact and importance of the proposed approach and tree boosting. XGBoost also provides scalability to the proposed system and accelerates the operation of inference. The scalability and faster inference from the XGBoost are due to several systems and algorithmic optimizations, including a novel tree learning algorithm.

Algorithm 3 iteratively summarizes the steps involved in the proposed approach, starting from site identification to the model training and building of the classifier. This algorithm also provides the adaptability to incorporate any existing forecasting and classification model and can be employed in different real-world scenarios apart from traffic volume detection only. The application areas include river water pollution detection, speeding detection, driver drowsiness detection, road condition monitoring *etc*. Here, the selection between these models (ARIMA or SVM) depends on various factors like the nature of the data, the forecasting horizon and the accuracy requirement. The decision to use a particular model is driven by its appropriateness for capturing the underlying patterns in the data and achieving optimal forecasting performance. In the proposed work, the choice between these models remains consistent based on the dataset's characteristics and the forecasting requirements. Additionally, the selection between ARIMA and SVM depends on the user's choice, as ARIMA requires more time for processing than SVM. These specific models were also selected due to their proven efficacy in handling data complexities and delivering reliable forecasts.

4.9 Conclusions

This chapter presented a comprehensive workflow for studying traffic-induced vibrations, covering instrumentation details, site selection, data collection and signal preprocessing. The tri-axial accelerometer setup (Section 4.3) facilitated accurate multi-directional vibration capture, while the LIDAR speed gun and Wi-Fi camera ensured precise speed measurements and event annotation. The selected sites (Section 4.3) reflected varied urban conditions, ranging from mid-block flat segments to speed hump scenarios, enabling a broad exploration of real-world vehicular interactions.

A unified filtering and segmentation pipeline (Section 4.4) was applied to all signals, ensuring drift removal, noise suppression and maximum-energy window extraction consistency. This standardized approach yielded high-quality data segments across multiple studies, including (i) speed hump vibration analysis (Section 4.5), (ii) reference emission (RVEL) and car-equivalent (PCVE) modeling (Section 4.6) and (iii) vehicle classification (Section 4.7) and (iv) traffic forecasting and route optimization strategies (Section 4.8). The studies underscore the methodological coherence and adaptability of the field data acquisition plan.

Moving forward, these datasets form the basis for multiple analytical frameworks such as classification, forecasting and route optimization, demonstrating the versatility of vibration-based insights in transportation engineering. The well-documented field measurements and preprocessing steps validate the data integrity and set a strong foundation for the advanced analyses detailed in subsequent chapters.